UPPSALA
UNIVERSITET

Digital Comprehensive Summaries of Uppsala Dissertations from the Faculty of Science and Technology 788

Density Functional Theory Studies of Small Supported Gold Clusters and Related Questions

What a Difference an Atom Makes

MARTIN AMFT

ACTA
UNIVERSITATIS
UPSALIENSIS
UPPSALA
2010

ISSN 1651-6214
ISBN 978-91-554-7946-6
urn:nbn:se:uu:diva-133246

Dissertation presented at Uppsala University to be publicly examined in Häggsalen, Ångströmlaboratoriet, Lägerhyddsvägen 1, Uppsala, Friday, December 17, 2010 at 13:15 for the degree of Doctor of Philosophy. The examination will be conducted in English.

Abstract

Amft, M. 2010. Density Functional Theory Studies of Small Supported Gold Clusters and Related Questions. What a Difference an Atom Makes. Acta Universitatis Upsaliensis. *Digital Comprehensive Summaries of Uppsala Dissertations from the Faculty of Science and Technology* 788. 85 pp. Uppsala. ISBN 978-91-554-7946-6.

During the last decades the specific manipulation of matter on the (sub-) nanometer scale, also known as nanoscience, became possible by technologies such as the scanning tunneling microscope. Nanocatalysts, i.e. catalytic active structures of up to a few nanometers in size, belong to this rather new class of materials. Unlike ordinary 'macroscopic' catalytic materials, the performance of nanocatalysts does not simply scale, for instance, with the surface to volume ratio of the active material.

In this Thesis model nanocatalysts are investigated by means of *ab-initio* density functional theory calculations.

In paper I, we explain the experimentally observed catalytic characteristics of small gold clusters, $Au_{1\text{-}4}$, on a regular magnesium oxide terrace towards the oxidation of carbon monoxide by thoroughly studying the adsorption of CO and O_2 on these clusters.

In the subsequent paper II, we study the feasibility of a catalytic water-mediated CO oxidation reaction on $Au_{1\text{-}4}$/MgO and find that this reaction mechanism is not assessable for $Au_{2,4}$/MgO and unlikely for $Au_{1,3}$/MgO.

Papers III and IV concentrate on the reactivity of clusters in the gas phase. Particularly, we focus on the relative stability of Au_{13} isomers and its potential for O_2 dissociation (paper III). We find the lowest energy isomers, which contain a triangular prism at their center surrounded by a ring of the remaining seven atoms, to be generally stable upon O_2 adsorption. The dissociation of O_2 at certain sites of Au_{13} is found to be exothermic.

In paper IV we performed scans of the Born-Oppenheimer potential energy surfaces of neutral and charged Cu_3, Ag_3, and Au_3 to explore the thermally excited vibrations of these trimers. While the Born-Oppenheimer surface of Cu_3 exhibits one fairly deep energy minimum, it is comparatively flat with two shallow minima in the case of Ag_3. Hence for Ag_3 there exist many thermally accessible geometries in a wide range of angles and bond lengths. For Au_3, two distinct energy minima appear, being well-separated by a barrier of 180 meV. Already at room temperature, we find bond lengths changes of up to 5% for the studied trimers. Choosing Au_3 as a case study for the changed reactivity of thermally excited modes, we find CO to bind up to 150 meV stronger to the excited cluster.

Gold deposited on graphene and graphite was observed to form larger aggregates. In paper V, we study the electronic structures, high mobility, and substrate-mediated clustering processes of $Au_{1\text{-}4}$ on graphene.

Already in the 1970s is was speculated that dispersion forces, i.e. van der Waals forces, significantly contribute to the adsorption energies of gold atoms on graphite. We accounted for van der Waals interactions in our density functional theory calculations (paper VI) and investigated the influence of these dispersion forces on the binding of copper, silver, and gold adatoms on graphene. While copper and gold show a mixed adsorption mechanism, i.e. chemical binding plus attraction due to the van der Waals forces, silver is purely physisorbed on graphene.

Keywords: Gold clusters, CO oxidation, graphene, spin-orbit coupling, van der Waals interactions, thermally excited vibrations

Martin Amft, Department of Physics and Astronomy, Materials Theory, Box 516, Uppsala University, SE-751 20 Uppsala, Sweden.

ISSN 1651-6214
ISBN 978-91-554-7946-6
urn:nbn:se:uu:diva-133246 (http://urn.kb.se/resolve?urn=urn:nbn:se:uu:diva-133246)

till min hustru Camilla und meine Eltern Elke und Ulrich Amft

List of Papers

This Thesis is based on the following papers, which are referred to in the text by their Roman numerals.
I performed all the VASP calculations, except for the DFT+D2 calculations in paper VI, as well as the vdW-DF calculations.
Furthermore, I wrote the manuscripts I, II, III, V, and VI and contributed to the writing of manuscript IV.

I **Catalytic activity of small MgO-supported Au clusters towards CO oxidation: A density functional study**
M. Amft and N. V. Skorodumova
Physical Review B **81**, 195443 (2010)

II **Does H_2O improve the catalytic activity of Au_{1-4}/MgO towards CO oxidation?**
M. Amft and N. V. Skorodumova
submitted to Journal of Catalysis (2010)

III **The relative stability of Au_{13} isomers and their potential for O_2 dissociation**
M. Amft and N. V. Skorodumova
in manuscript

IV **Thermally Excited Vibrations in Copper, Silver, and Gold Trimers and Enhanced Binding of CO**
M. Amft, T. Edvinsson, and N. V. Skorodumova
submitted to Journal of the American Chemical Society (2010)

V **Small gold clusters on graphene, their mobility and clustering: A DFT study**
M. Amft, B. Sanyal, O. Eriksson, and N. V. Skorodumova
submitted to Physical Review B (2010)

VI **Adsorption of Cu, Ag, and Au atoms on graphene including van der Waals interactions**
M. Amft, S. Lebègue, O. Eriksson, and N. V. Skorodumova
submitted to Physical Review B (2010)

The following papers are co-authored by me but are not included in this Thesis.

- **Growth of the first water layer on rutile TiO_2(110)**
  L. E. Walle, M. Amft, D. Ragazzon, A. Borg, P. Uvdal, N. V. Skorodumova, and A. Sandell
  in manuscript (2010)
- **Hidden order in URu_2Si_2 originates from Fermi surface gapping induced by dynamic symmetry breaking**
  S. Elgazzar, J. Rusz, M. Amft, P. M. Oppeneer, and J. A. Mydosh
  Nature Materials **8**, 337 (2009)
- **Magnetic Circular Dichroism in Two-Photon Photoemission**
  K. Hild, J. Maul, G. Schönhense, H. J. Elmers, M. Amft, and P. M. Oppeneer
  Physical Review Letters **102**, 057207 (2009)
- **First-principles calculations of optical and magneto-optical properties of $Ga_{1-x}Mn_xAs$ and MnAs**
  M. Amft, T. Burkert, B. Sanyal, and P. M. Oppeneer
  Physica B: Physics of Condensed Matter **404**, 3782 (2009)
- **Calculated magneto-optical Kerr spectra of the half-Heusler compounds AuMnX (X = In, Sn, Sb)**
  M. Amft and P. M. Oppeneer
  Journal of Physics: Condensed Matter **19**, 315216 (2007)

Contents

1. Introduction

Approximately one out of one thousand one hundred and fifty seven Germans is a physicist. I am one of them.

My decision to study physics dates back to my teens. After convincing my parents of this for them rather strange idea, I received all their support I could ask for during the years. In secondary school, I made my first steps into the field of computational physics, when I participated in a nation wide science contest for pupils. For that purpose, my physics teacher, Maik Burgemeister, allowed me to run my simulation on all the brand new 100 MHz Pentium PCs of the school's computer lab in parallel.

I enrolled to study physics, and additionally some philosophy and extra mathematics, at the Friedrich-Schiller-University in Jena, Germany, in 2000. After six semesters, I moved to Uppsala for one year to study as an exchange student. I obtained my diploma in physics from the Friedrich-Schiller-University in Jena for a thesis on 'Superconducting Qubits as an example of dissipative quantum systems' under the supervision of PD Dr. Wolfram Krech at the Institute of Solid State Physics in 2005. Through this I came to work, somewhat unintentionally, in solid state physics. When I was looking for a PhD project to continue my studies, it was rather natural to stay in this exciting and diverse branch of physics.

This Thesis is the result of my research years in the materials theory group of Prof. Olle Eriksson. Initially, I studied the electronic structures and magneto-optics of $d-$ and $f-$electron systems under the supervision of Prof. Peter M. Oppeneer, which led to my Licentiate degree.

In autumn 2008, I changed the focus of my research. Still using computational methods, I started studying a number of problems within the fields of surface science and cluster physics under Dr. Natalia V. Skorodumova's supervision.

Both fields have a long history, almost 100 years in the case of surface science. However, the specific manipulation of matter on the (sub-)nanometer scale, also known under its popular name nanoscience, first became feasible during the last decades. A famous example, are the three letters I, B, and M 'written' with a scanning tunneling microscope as a pen, 35 xenon atoms as ink, and a nickel surface as paper. On this length scale, matter is solely governed by the laws of quantum mechanics and shows often unexpected properties. The layman might even call them counterintuitive.

The nanometer-sized systems, I became mostly interested in, are so-called nanocatalysts. In contrast to ordinary catalysts, nanocatalysts do not follow simple scaling rules, such as: 'increase the surface to volume ratio and your catalytic material will do a better job speeding up your chemical reaction.' Instead, every single atoms counts in the nanocatalyst, especially in the smallest systems, that I studied.

The results of my last two research years are the content of this Thesis. Although not formally divided, it consists of two parts: an introduction (Chapters 2 to 4) and a summary of my projects in Chapter 5. The latter chapter is self-contained, such that the impatient reader can immediately delve into the contents of papers I - VI, which are also attached to the printed version of this Thesis. Still, it was my intention to make the following introduction chapters also a worthwhile read for those, who are already experts in quantum mechanics and solid state theory.

With hindsight, it is often easy to see the necessities, which created the theories and methods, we are using today. In the next chapter (Chap. 2), I briefly tell the fascinating story of our current understanding of condensed matter in terms of its electronic structure.

A quantum mechanical description of the condensed phase was developed until the beginning of the 1960s. However, the future development of this particular branch of physics might have looked rather bleak to contemporary physicists. The reason for this outlook was mainly of practical nature. The than available methods did not allow to accurately and efficiently calculate many-electron systems, in spite of computer's becoming increasingly capable. A real break-through started in the middle of the 1960s, when the foundation of the so-called density functional theory was created, see Chapter 3.

The basics of this density functional theory are presented in Section 3.1. A number of necessary approximations, especially to the unknown exchange-correlation functional, are crucial for applying this theoretical framework. Two approximations, that go beyond the original local density approximation, are the content of Section 3.2, i.e. the generalized-gradient approximation and the addition of van der Waals interactions to the correlation energy.

There exists a wide range of implementations of the density functional theory. In Chapter 4, the so-called projected augmented-wave method and its implementation in the Vienna Ab-Initio Simulation Package (VASP) are introduced. I used this implementation for my calculations in papers I - VI.

Section 5.2 gives a short introduction to nanocatalysis. The calculation and understanding of model nanocatalysts, especially small gold clusters, is the theme of papers I to IV.

Graphene, which enjoyed an increasing popularity during recent years, was used as a substrate for small gold clusters and coinage metal atoms in papers V and VI, respectively. A summary of these results is compiled in Section 5.3.

In the final chapter (Chap. 6), I attempt to identify a number of interesting problems, that could be addressed as a continuation of the projects contained in this work.

It is my hope that you will enjoy reading this Thesis as much as I enjoyed writing it!

Uppsala, October 2010

Martin Amft

2. A brief history of condensed matter theory

Working in academia has many enjoyable aspects to it. One of them is the connection of my profession with some of my spare-time interests. History, especially the history of sciences, belongs to these overlapping interests. To know who answered which question how and for what reason is essential for my understanding of the subject. Therefore, I will give a concise history of our current understanding of the electronic structure of the condensed matter, ranging from the early scientific speculations about the atom to the concrete methods used in this Thesis.

As a layman to this field, it is not my ambition to compete with trained historians of science. Instead I will describe the development until the mid-1930s in detail, including references to the original works for further reading. After that time the subject becomes very diverse and I will focus on the topics that are most relevant for this Thesis.

2.1 You were right, Mr. Dalton

The chemist J. Dalton introduced the theory of atoms in the early 19th century, summarized in his book *A New System Of Chemical Philosophy* published in 1808. He assumed that each element consists of indivisible and identical atoms of a certain weight. During chemical reactions, atoms simply change the way they are grouped together. This is called the law of multiple proportions. Although being successfully used in chemistry, the atom theory was only a working hypothesis for almost 100 years to come.

By the end of the 19th century, all then known physical phenomena could be explained within the theory-framework of classical and statistical mechanics, thermodynamics, and electrodynamics with sufficient accuracy.

A deeper understanding of the structure of matter did not start to arise before K. F. Braun's invention of the cathode-ray tube in 1897 [1]. In the same year, J. J. Thomson started to measure the ratio of the elementary charge to the electron's mass, e/m_e, with increasing accuracy using a cathode-ray tube [2–4]. From his discovery of the electron he developed until 1904 the so-called 'plum-cake model', the first model of the atom's inner structure [5].

Despite the collection of a vast amount of circumstantial data by chemists and physicists during the end of the 19th century, direct proof of the atoms very existence was still missing. In his third publication during his *annus*

mirabilis in 1905, A. Einstein quantitatively related the Brownian motion of suspended particles to the collisions with surrounding molecules [6]. J. Perrin's work [7] supplied the necessary experimental evidence to Einstein's theory, finally establishing the existence of atoms as a scientific fact. This newly gained knowledge also allowed the chemists of the time to dismiss competing theories about the structure of matter.

From then onwards, models of the atoms inner structure were developed with an increasing pace. In 1909, H. Geiger, E. Marsden, and E. Rutherford concluded from their scattering experiments of α-particles on thin gold foils that atoms contain a positively charged nucleus, which carries almost the whole mass of the atom [8]. Two years later Rutherford published his solar system model of the atom, i.e. electrons that revolve on elliptical orbitals around the central nucleus [9].

The model's most significant shortcoming was its inability to correctly describe the absorption and emission of light. N. Bohr overcame this particular problem by adding three postulates to the idea of a solar system-like atom [10–12]

1. there exist stable, circular electron orbitals around the nucleus,
2. absorption and emission of light is possible through quantum-leaps of the electron from one stable orbital to another,
3. stable orbitals are defined by their quantized angular momentum $L = n\hbar$, with n being an integer and $\hbar$ Planck's constant divided by 2π.

Although Bohr's atom model was refined by A. Sommerfeld, i.e. by refining the quantization rules [13, 14], a derivation of these *ad hoc* hypotheses was only possible after the development of a new physical theory of the motion of microscopical particles, i.e. quantum mechanics, see Sec. 2.3.

2.2 A detour: From dust to dawn

In the last two decades of the 19th century, physical chemists started to apply thermodynamics to their field. Motivated by these successes, a younger generation, such as I. Langmuir [1], started also to use statistical mechanics in physical chemistry in the early 20th century.

[1] Langmuir gave an outlook where this process might lead, from Ref. [15]: 'As yet, apparently, very few chemists have awakened to the wonderful opportunities that lie open to them on all sides when they attack the problems of chemistry by the new methods [statistical mechanics plus atom theory] which the physicists have developed. The physicist, on the other hand, is gradually beginning to extend his investigations into the field of the chemist and we may hope, if the chemist will but meet him half way, that there will result a new physical chemistry which will have an even more far-reaching effect on our ordinary chemical conceptions than has the physical chemistry of the last decades.'

The emergence of surface science, especially surface chemistry, is closely related to Langmuir's early work on the behavior of low-pressure gases in light bulbs. In 1913 he started investigating bulbs filled with hydrogen gas and found that it dissociates. He correctly deduced that hydrogen atoms adsorb on the glass surface of the bulb [16]. In subsequent works, he studied the clean-up of oxygen and nitrogen from these lamps and the blackening of their inner glass surface[2], which Langmuir explained with a heterogeneous catalytic reaction taking place on the heated tungsten filament [17, 18].

From contemporary x-ray diffraction experiments on crystals[3], carried out by M. Laue [21] and W. L. Bragg [22], scientists had a qualitative understanding of the surface structures of solids and how gas molecules adsorb on these surfaces.

Langmuir was the first to quantitatively investigate the adsorption of gas molecules on the surfaces of solids and how they order to form the first monolayer [23]. Shortly afterwards he also developed a quantitative model for heterogeneous catalytic reactions, i.e. the reaction of two pre-adsorbed species on neighboring sites on a solid surface, that is still in use today [24].

2.3 Gold rush in quantum land

In Sec. 2.1, we already encountered Planck's constant ($h = 6.626 \cdot 10^{-34}$ J s), while discussing Bohr's atom model. M. Planck felt forced to introduce the *ad hoc* hypothesis that the emission and adsorption of electromagnetic radiation by matter is quantized by multiples of h in order to correctly describe the black body radiation [25].

P. Lenard discovered the photoelectric effect [26] in 1902, which Einstein could explain by assuming that all electromagnetic radiation consists of light quanta with an energy $E = h\nu$ [27]. A. H. Compton used Einstein's concept of a photon to develop a quantum theory for the scattering of x-rays and γ-rays on light elements [28].

When W. Gerlach and O. Stern studied a beam of neutral silver atoms that passed through a magnetic field, they detected two separated spots on their screen - the first experimental evidence for another quantized quantity, the electron spin, was found. They concluded that each silver atom must carry a magnetic moment, which can only point in two distinct directions, and that this moment is an inherent property of their outer electron [29–31].[4] These

[2] So, one can say: from the "dust" in light bulbs originated the dawn of surface science.

[3] Note that the mathematician A. Bravais already derived the 14 crystallographic structures in the middle of the 19th century [19, 20].

[4] Also in 1921 A. H. Compton speculated about a 'possible magnetic polarity of free electrons', i.e. the electron spin [32]. I can not answer, if Compton knew of Stern and Gerlach's first two publications [29, 30].

paramount experimental evidences made it obvious that the known classical laws of physics fail at the microscopic scale.

Within a few years only, two seemingly different formulations of quantum mechanics were developed until the mid-1920s: the so-called matrix mechanics of W. Heisenberg, M. Born, and P. Jordan [33–35] and E. Schrödinger's wave mechanics [36–39].

Schrödinger based his theory on the earlier work of L. de Broglie [40], i.e. the wave-particle duality of matter. He found Equ. (2.1), named after him, that describes the dynamics of a quantum system as a function of kinetic ($-\hbar^2/2m\Delta$) and its potential (V) energy

$$i\hbar\frac{\partial}{\partial t}\Psi(\vec{r},t) = \left(-\frac{\hbar^2}{2m}\Delta + V(\vec{r})\right)\Psi(\vec{r},t). \tag{2.1}$$

Schrödinger was the first to show the equivalence of his formulation of quantum mechanics to that of Born, Heisenberg, and Jordan [41].

P. M. A. Dirac formulated his non-relativistic theory of quantum mechanics shortly afterwards and showed that it includes the matrix and the wave mechanics as special cases [42]. Still, a stringent proof of the equivalence of the matrix and the wave mechanic formalisms was first published in 1932 by the mathematician J. von Neumann [43].

None of these three formulations of quantum mechanics includes the spin. By considering it as an additional degree of freedom of the wave function, i.e. $\vec{\Psi}$ becomes a two-dimensional vector for the two spin channels, W. Pauli integrated the electron spin into the Schrödinger equation (2.1) [44]:

$$i\hbar\frac{\partial}{\partial t}\vec{\Psi}(\vec{r},t) = \left(\frac{(\vec{p}-e\vec{A})^2}{2m} + e\varphi\right)\vec{\Psi}(\vec{r},t) - g\frac{e\hbar}{2mc}\frac{\vec{\sigma}}{2}\cdot\vec{B}\vec{\Psi}(\vec{r},t), \tag{2.2}$$

with $\vec{p}$ being the momentum operator, $\vec{A}$ the vector potential, ϕ the electrical potential, and $\vec{B}$ the magnetic field. The three components of $\vec{\sigma}$ are the well-known 2×2 Pauli matrices.

Less than one year later, Dirac found the correct relativistic formulation of quantum mechanics, Ref. [45, 46]:

$$i\frac{\partial}{\partial t}\vec{\Psi} = \left(\vec{\alpha}\cdot(\vec{p}-e\vec{A}) + e\varphi + \gamma^0 m\right)\vec{\Psi}. \tag{2.3}$$

As in the Pauli equation (2.2), $\vec{p}$ is the momentum operator, $\vec{A}$ is the vector potential, and ϕ is the electrical potential. The components of $\vec{\alpha}$ are given by $\alpha^i = \gamma^0\gamma^i$, with γ^j being the 4×4 Dirac matrices. Similarly to the Schrödinger equation (2.1), Equ. (2.3) is of first order in time. However, as

a relativistic equation, the Dirac equation has to treat time and space in a symmetric fashion. Therefore it is of first order in space as well.

With the Dirac equation (2.3), it is in principle possible to calculate all physical and chemical phenomena that are determined by the electronic structure of matter.[5]

So, during the 1920s physicists claimed a whole new world and developed the basis for most of today's physics.[6] Nonetheless, the reader might be reminded that there still remain open questions on certain consequences of quantum mechanics that physicists and chemists try to settle. Just to name three: entanglement, decoherence, and the measurement process.

2.4 Beyond hydrogen

Although, finding exact solutions of the Schrödinger and the Dirac equation, Eqs (2.1) and (2.3) respectively, are practically impossible for systems more complicated than the hydrogen atom or the helium cation, we will see in the following subsections how quantum mechanics was successfully applied to crystalline solids.

2.4.1 New wine in old bottles

Since quantum theory was originally developed to describe the electronic structure of atoms, it was only natural to first apply the new theory to this type of many-body problems, e.g. to study the coupling of angular and spin moments by S. Goudsmit and G. E. Uhlenbeck [48].

Trying to understand the spectra of atoms, Pauli formulated the exclusion principle for electrons already in 1925 [49]. E. Fermi generalized this concept and formulated an equation of state for a system of non-interacting particles [50]. The first attempts to bridge the gap between the physics of single atoms and the physics of solid bodies were again undertaken by Pauli. He extended Fermi's equation of state to gas atoms with an angular momentum in order to describe the paramagnetism in gases. By considering the conduction electrons of, for instance, alkali metals as a degenerated ideal gas, Pauli could even qualitatively describe the paramagnetism in these metals [51].

[5]The reader might be familiar with Dirac's alleged statement '..the rest, is chemistry.' This reductionistic view, which is not unfamiliar amongst physicists, was challenged, for instance, by P. W. Andersson in Ref. [47]. Therein he argues for the existence of a hierarchy of the natural phenomena, reflected in a hierarchical structure of science, where 'at each level of complexity entirely new properties appear, and the understanding of the new behaviors requires research which I think is as fundamental in its nature as any other.'

[6]Roughly the same time span miners needed some seven decades earlier to extract most of California's gold.

Sommerfeld re-derived the known expressions for the conductivity, surface phenomena, different thermoelectrical, galvanomagnetic and thermomagnetic effects in metals from Fermi statistics [52,53]. But he noticed himself that the concept of the mean free path of electrons in solid bodies was not sufficiently well developed and needed to be refined within the framework of wave mechanics. Especially the scattering of electrons on the metal ions was not included in his theory of metals.

2.4.2 What's so special about electrons in crystals?

With Sommerfeld's theory of metals at hand, how can one incorporate the crystal structure into the wave mechanical description of the electrons in a metal? This question was almost simultaneously and independently addressed by a number of young physicists H. Bethe (student of Sommerfeld) [54], E. E. Witmer and L. Rosenfeld [55] (students of Born), and F. Bloch [56] (student of Heisenberg) in the late 1920s.

In the following Bloch's derivation of the theorem, named after him, will be derived. He started from the time-independent Schrödinger equation (2.1) for an electron in the periodic electrical potential of a crystal

$$V(\vec{r}) = V(\vec{r} + g_1\vec{a} + g_2\vec{b} + g_3\vec{c}). \tag{2.4}$$

Here, $r_G = g_1\vec{a} + g_2\vec{b} + g_3\vec{c}$ (g_1, g_2, g_3 integer) is an arbitrary lattice vector. In order to solve a Schrödinger equation (2.1) with a potential of the form Equ. (2.4), Bloch assumed periodic boundary conditions, i.e. the whole lattice is build up by repeating the parallelepiped defined by $(G_1\vec{a}, G_2\vec{b}, G_3\vec{c})$ in all three spatial dimensions. These boundary conditions allowed him to show that a wave function of the form

$$\Psi_{klm}(x,y,z) = e^{2\pi i\left(\frac{kx}{aG_1} + \frac{ly}{bG_2} + \frac{mz}{cG_3}\right)} u_{klm}(x,y,z) \tag{2.5}$$

solves Equ. (2.1). Here, a,b,c is the periodicity of the potential in Equ. (2.4) and k,l,m integer numbers defined by the wave vector.

Bloch commented on Equ. (2.5), from Ref. [56]: 'Since one can always divide the eigenfunction into a factor $e^{2\pi i\left(\frac{kx}{aG_1} + \frac{ly}{bG_2} + \frac{mz}{cG_3}\right)}$ and a rest, that only contains the periodicity of the lattice, one could descriptively say that we are dealing with plain de Broglie waves which are modulated by the lattice.' Hence the main physical conclusion to be drawn from the Bloch Theorem Equ. (2.5) is that electrons form bands in a periodic potential, allowing the electrons to move freely through a perfect lattice and only scatter on impurities and displaced ions, i.e. displaced due to thermal vibrations.

Although Equ. (2.5) was also derived by Witmer and Rosenfeld [55], it was Bloch who substantially build upon this result, deriving, for instance,

expressions for the conductivity and the specific heat of the electrons in a crystal [56].

From here on, it was possible to derive theories for a wide range of phenomena in solids by combining Bloch's electron band theory with the Pauli principle and Fermi's equation of state. R. Peierls was one of the pioneers in this field. He investigated the Hall effect [57] and the electrical and thermal conductivity of metals [58]. He recognized that each eigenstate (2.5) can only hold one electron per spin state and unit cell.

The classification of crystals into metals, semiconductors, and insulators based on the electron band theory was introduced by A. H. Wilson in 1931 [59, 60].

The beginning of quantitative calculations of the electronic band energies date back to 1933 when E. Wigner and F. Seitz calculated the lowest energy level and lattice constant of sodium [61, 62]. The first energy band was calculated by J. C. Slater by using the methods developed by Wigner and Seitz [63].

Although these early calculations took the Pauli principle into account, they neglected electron-electron interactions, which are not part of the Bloch theorem, Equ. (2.5). The full hamiltonian of a system of N_e electrons and N_I ions, which takes ion-ion, ion-electron, and electron-electron interactions into account, can be written as [64]:

$$\begin{aligned} \hat{H} &= -\frac{\hbar^2}{2m_e}\sum_i \nabla_i^2 + \sum_{i,I}\frac{Z_I e^2}{|\vec{r}_i - \vec{R}_I|} + \frac{1}{2}\sum_{i\neq j}\frac{e^2}{|\vec{r}_i - \vec{r}_j|} \\ &- \sum_I \frac{\hbar^2}{2M_I}\nabla_I^2 + \frac{1}{2}\sum_{I\neq J}\frac{Z_I Z_J e^2}{|\vec{R}_I - \vec{R}_J|}. \end{aligned} \tag{2.6}$$

Here, lower case indices label electron quantities and upper case indices those of the ions.

As a first simplification of Equ. (2.6) one can introduce the so-called Born-Oppenheimer, or adiabatic, approximation. For many purposes in solid state physics, it is justified to neglect the kinetic energy term of the nuclei, due to their higher masses. This gives a many-body hamiltonian of the form

$$\hat{H} = \hat{T} + \hat{V}_{\text{ext}} + \hat{V}_{\text{int}} + E_{\text{II}}, \tag{2.7}$$

where atomic units, i.e. $\hbar = m_e = e = 1$, were used. The last term E_{II} is simply the classical Coulomb interaction of the nuclei. From Equ. (2.6), using the Born- Oppenheimer approximation, one identifies the kinetic energy operator and the electron-electron interaction as

$$\hat{T} = -\frac{1}{2}\sum_i \nabla_i^2 \qquad \text{and} \qquad \hat{V}_{\text{int}} = \frac{1}{2}\sum_{i\neq j}\frac{1}{\vec{r}_i - \vec{r}_j}. \tag{2.8}$$

Since the motion of the nuclei is assumed to be slow compared to the electrons', the electron-nuclei interaction takes the form of electrons moving in a fixed external potential

$$\hat{V}_{\text{ext}} = \sum_{i,I} V_I(|\vec{r}_i - \vec{R}_I|). \tag{2.9}$$

Further external electric or magnetic potentials can easily be included in Equ. (2.7) by adding appropriate terms to Equ. (2.9).

Eigenstates of the many-body hamiltonian Equ. (2.7) are saddle points or minima of the total energy expectation value

$$\begin{aligned} E &= \frac{\langle\Psi|\hat{H}|\Psi\rangle}{\langle\Psi|\Psi\rangle} \\ &= \langle\hat{T}\rangle + \langle\hat{V}_{\text{ext}}\rangle + \int \mathrm{d}^3 V_{\text{ext}}(\vec{r})\, n(\vec{r}) + E_{II}, \end{aligned} \tag{2.10}$$

where $\Psi = \Psi(\vec{r}_1, \vec{r}_2, \ldots, \vec{r}_{N_e})$ are the many-body wave functions of the electrons and $n(\vec{r})$ is the expectation value of the density operator $\hat{n}(\vec{r}) = \sum_{i=1,N_e} \delta(\vec{r} - \vec{r}_i)$

$$n(\vec{r}) = \frac{\langle\Psi|\hat{n}(\vec{r})|\Psi\rangle}{\langle\Psi|\Psi\rangle} \tag{2.11}$$

$$= N_e \frac{\int \mathrm{d}^3 r_2 \cdots \mathrm{d}^3 r_{N_e} \sum_\sigma |\Psi(\vec{r}, \vec{r}_2, \ldots, \vec{r}_{N_e})|^2}{\int \mathrm{d}^3 r_1\, \mathrm{d}^3 r_2 \cdots \mathrm{d}^3 r_{N_e} |\Psi(\vec{r}_1, \vec{r}_2, \ldots, \vec{r}_{N_e})|^2}. \tag{2.12}$$

Note that the spin was implicitly included into the coordinates $\vec{r}_i$ of the wave function Ψ. By minimizing the total energy E of the many-body system, Equ. (2.10), with respect to all the parameters in Ψ, and observing the particle symmetry and all necessary conservation laws, one can, in principle, find the ground state wave function Ψ_0.

Albeit using the Born-Oppenheimer approximation, solutions to a Schrödinger equation with a many-body hamiltonian Equ. (2.7) have to be approximative for all but the most simple cases. Especially the electron-electron interactions $\hat{V}_{\text{int}}$ are a challenge to treat with sufficient accuracy. The following chapter (Chap. 3) on density functional theory will present a reformulation of the many-body problem and approximations of the electron-electron interactions. These will allow for finding numerical solutions for the ground state density, energy, and derived quantities.

3. Our way to solve the too-many-bodies problem

Even before the rise of quantum mechanics, efforts were undertaken to calculate the spectra of atoms other than hydrogen. Starting from Sommerfeld's refined atom model [13, 14] there were various attempts to find effective atomic potentials by fitting empirical data, e.g. E. Fues [65, 66].

Among the first to take a reductionistic approach, i.e. to derive energy functionals to approximate the electronic structure of atoms from theory alone, were L. H. Thomas [67] and E. Fermi [68], here in its form taken from Ref. [64],

$$\begin{aligned} E_{\mathrm{TF}}[n] &= C_1 \int \mathrm{d}^3 r\, n(\vec{r})^{5/3} + \int \mathrm{d}^3 r\, V_{\mathrm{ext}}(\vec{r})\, n(\vec{r}) \\ &+ C_2 \int \mathrm{d}^3 r\, n(\vec{r})^{4/3} + \frac{1}{2} \int \mathrm{d}^3 r\, \mathrm{d}^3 r' \frac{n(\vec{r})\, n(\vec{r}')}{|\vec{r} - \vec{r}'|}, \end{aligned} \tag{3.1}$$

where the first term is a local approximation of the kinetic energy ($C_1 = \frac{3}{10}(3\pi^2)^{2/3}$), the third term is the local exchange ($C_2 = -\frac{3}{4}(\frac{3}{\pi})^{1/3}$), V_{ext} is the external potential due to the nuclei, and the last term is the classical Hartree energy. Note that correlations are neglected in this original density functional theory.

3.1 Density functional theory, exact and solvable - in principle

It took almost four decades after the original work of Thomas and Fermi until an exact density functional theory of many-body systems was developed by P. Hohenberg, W. Kohn, and L. J. Sham [69, 70]. We cite the theorems of their theory in the form given in Ref. [64]:

Theorem I: For any system of interacting particles in an external potential $V_{\mathrm{ext}}(\vec{r})$, the potential $V_{\mathrm{ext}}(\vec{r})$ is determined uniquely, except for a constant, by the ground state particle density $n_0(\vec{r})$.

Corollary I: Since the hamiltonian is thus fully determined, except for a constant shift of the energy, it follows that the many-body wave

functions for all states (ground and excited) are determined. Therefore all properties of the system are completely determined given only the ground state density $n_0(\vec{r})$.

Theorem II: A universal functional for the energy $E[n]$ in terms of the density $n(\vec{r})$ can be defined, valid for any external potential $V_{\text{ext}}(\vec{r})$. For any particular $V_{\text{ext}}(\vec{r})$, the exact ground state energy of the system is the global minimum value of this functional, and the density $n(\vec{r})$ that minimizes the functional is the exact ground state density $n_0(\vec{r})$.

Corollary II: The functional $E[n]$ alone is sufficient to determine the exact ground state energy and density.

In mathematical terms, theorem II can be expressed as

$$E[n] = \int \mathrm{d}^3 r\, V_{\text{ext}}(\vec{r})\, n(\vec{r}) + \frac{1}{2} \int \mathrm{d}^3 r\, \mathrm{d}^3 r' \frac{n(\vec{r})\, n(\vec{r}')}{|\vec{r} - \vec{r}'|} + F_{\text{HK}}[n], \tag{3.2}$$

where $F_{\text{HK}}[n]$ is an universal functional of the electron density [69]. The challenge lies in finding an approximation for $F_{\text{HK}}[n]$, which describes with sufficient accuracy the exchange and correlation energy of the interacting many-particle system of a given density $n(\vec{r})$.

The so-called Kohn-Sham ansatz, Ref. [70], assumes that $F_{\text{HK}}[n]$ can be written as

$$F_{\text{HK}}[n] = T_s[n] + E_{xc}[n], \tag{3.3}$$

where $T_s[n]$ is the kinetic energy of a system of non-interacting particles and $E_{xc}[n]$ is the exchange and correlation energy of a system of interacting particles. Kohn and Sham further assumed that the exchange-correlation energy

$$E_{xc}[n] = \int \mathrm{d}^3 r\, n(\vec{r}) \varepsilon_{xc}[n], \tag{3.4}$$

with $\varepsilon_{xc}[n]$ parametrized from the exchange and correlation energy of a homogenous electron gas, is a sufficiently good approximation for a system of interacting particles with slowly varying density $n(\vec{r})$. This is the so-called local density approximation (LDA).

In summary, the Kohn-Sham energy functional is given by

$$\begin{aligned} E_{\text{KS}}[n] = & - \frac{1}{2}\nabla_s^2 + \int \mathrm{d}^3 r\, V_{\text{ext}}(\vec{r})\, n(\vec{r}) \\ & + \frac{1}{2} \int \mathrm{d}^3 r\, \mathrm{d}^3 r' \frac{n(\vec{r})\, n(\vec{r}')}{|\vec{r} - \vec{r}'|} + \int \mathrm{d}^3 r\, n(\vec{r}) \varepsilon_{xc}[n] \end{aligned} \tag{3.5}$$

$$= \quad T_s[n] + E_{\text{ext}}[n] + E_{\text{Hartree}}[n] + E_{\text{xc}}[n] \tag{3.6}$$

and the corresponding, spin-dependent, hamiltonian

$$\hat{H}^{\sigma}_{\text{KS}}(\vec{r}) = -\frac{1}{2}\nabla_s^2 + V^{\sigma}_{\text{KS}}(\vec{r}), \tag{3.7}$$

where the effective potential is derived from varying the energy terms with respect to the density

$$V^{\sigma}_{\text{KS}}(\vec{r}) = V_{\text{ext}}(\vec{r}) + \frac{\delta E_{\text{Hartree}}}{\delta n(\vec{r},\sigma)} + \frac{\delta E_{\text{xc}}}{\delta n(\vec{r},\sigma)}. \tag{3.8}$$

With the Kohn-Sham hamiltonian Equ. (3.7), a Schrödinger-like equation for the auxiliary system of non-interacting particles can be written as

$$(\hat{H}^{\sigma}_{\text{KS}}(\vec{r}) - \varepsilon_i^{\sigma})\psi_i^{\sigma}(\vec{r}) = 0. \tag{3.9}$$

Since the effective potential, $V^{\sigma}_{\text{KS}}(\vec{r})$, is a function of the particle density, the Kohn-Sham equation (3.9) must be solved self-consistently. Still, solving this system of one-electron Schrödinger-like equations for the $\psi_i^{\sigma}(\vec{r})$ is much easier than solving the original many-body problem in Equ. (2.7). One should keep in mind that all the many-body properties of the system are now concentrated in the approximation of the exchange-correlation energy functional $E_{\text{xc}}[n]$.

3.2 Two steps up on Jacob's ladder

As indicated at the beginning of this chapter, there are two distinct approaches for constructing exchange-correlation energy functionals, $E_{\text{xc}}[n]$: an empirical and a reductionistic one. A widely popular class of (semi-)empirical functionals are the so-called hybrid-functionals, such as the B3LYP functional [71],

$$E_{xc}^{\text{B3LYP}} = E_{xc}^{\text{LDA}} + a_0(E_x^{\text{exact}} - E_x^{\text{LDA}}) + a_x\Delta E_x^{\text{B88}} + a_c\Delta E_c^{\text{PW91}}, \tag{3.10}$$

where a_0, a_x, and a_c are fitting parameters, optimized for empirical data of a selection of atoms and molecules. E_x^{exact} is the exact exchange energy and ΔE_x^{B88} (ΔE_c^{PW91}) are exchange (correlation) gradient corrections [72, 73].

J. P. Perdew and K. Schmidt wrote an informative road-map about the reductionistic approach [74], titled 'Jacob's ladder[1] of density functional

[1] 'Jacob left Beer-sheba and went toward Haran. He came to a certain place and stayed there for the night, because the sun had set. Taking one of the stones of the place, he put it under his head

approximations for the exchange-correlation energy', see also Fig. 3.1. In this scheme, the above mentioned local density approximation, Equ. (3.4), and the generalized gradient approximation (GGA) are the lowest, best understood rungs of the ladder. Higher rungs become more and more computational expensive, e.g. by incorporating exact exchange, and are less well understood [74].

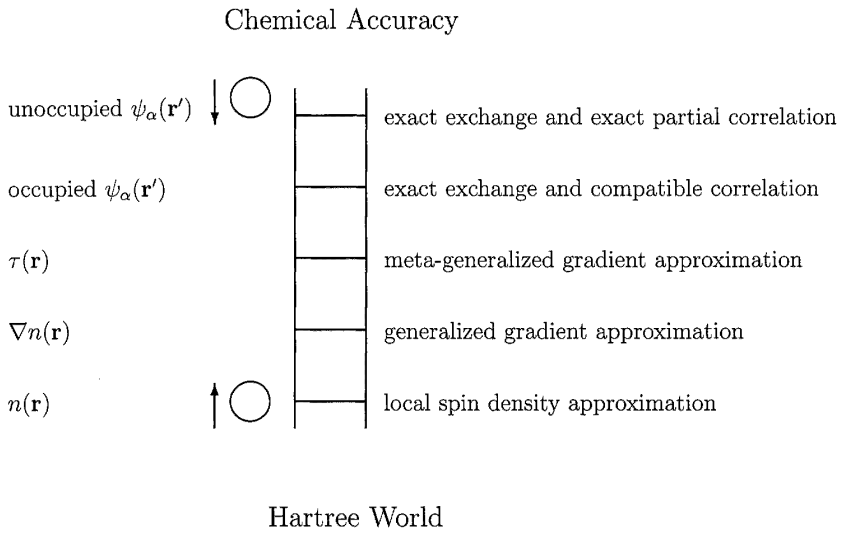

Figure 3.1: From Ref. [74]: 'Jacob's ladder of density functional approximations. Any resemblance to the Tower of Babel is purely coincidental. Also shown are angels in the spherical approximation, ascending and descending. Users are free to choose rungs appropriate their accuracy requirements and computational resources. However, at present their safety can be guaranteed only on the two lowest rungs.'

In most of our projects, we used a generalized gradient approximation to the exchange-correlation energy, which is presented in the following section 3.2.1. For our study of the adsorption of coinage metal atoms on graphene, manuscript VI, we climbed Jacob's ladder up one more step and also included van der Waals interactions in our calculations by two different implementations. The implementation used by me is described in greater detail in section 3.2.2 below.

---

and lay down in that place. And he dreamed that there was a ladder set up on the earth, the top of it reaching to heaven; and the angels of God were ascending and descending on it.' Genesis 28:10-12

3.2.1 Generalized gradient approximations

While the local density approximation, Equ. (3.4), as its name suggests, determines the contribution to the exchange-correlation energy within a volume element dV from the local electron density within dV only, generalized gradient approximations (GGA) also take the change of the electron density in dV into account [75, 76]:

$$E_{\mathrm{xc}}^{\mathrm{GGA}}[n] = \int \mathrm{d}^3 r\, n(\vec{r})\, \varepsilon_{\mathrm{xc}}^{\mathrm{GGA}}(n(\vec{r}), \nabla n(\vec{r})). \tag{3.11}$$

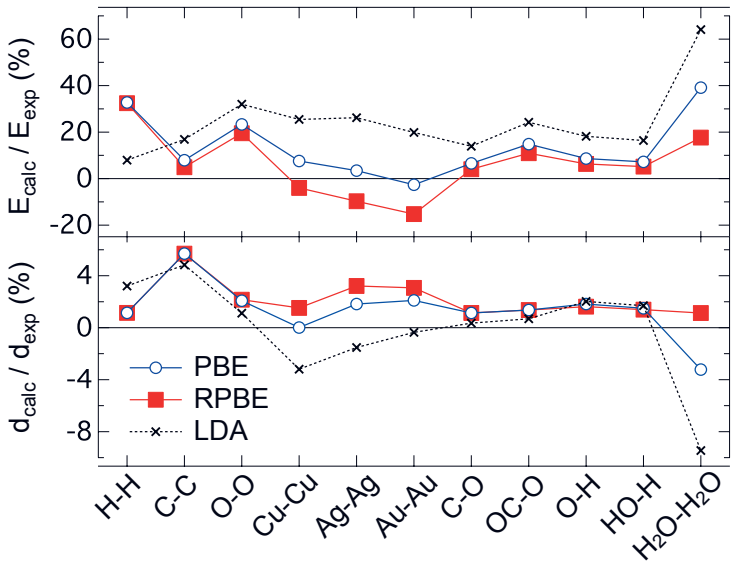

Figure 3.2: Performance in predicting bond dissociation energies (upper panel) and bond length (lower panel) of LDA (crosses) compared to PBE (open circles) and RPBE (full squares). The relevant bonds are indicated in the labels on the x-axis. The experimental values are taken from [77], except for d[Ag_2] [78] and d[$(H_2O)_2$] [79]. Note that H_2 has to be calculated without spin-polarization in GGA.

There exists quite a number of different parameterizations of GGA. For the systems we studied, we found the parameterizations of the exchange-correlation energy by Perdew, Burke, and Ernzerhof (PBE) [80] and its revised version by Hammer, Hansen, and Nørskov (RPBE) [81] to be most appropriate. Semi-local density contributions are included in both parametrizations by functional extensions to the LDA exchange and correlation energy densities, which depend on fundamental constants only. The difference of PBE and RPBE lies only in the functional form of $F_x(s)$ used in the exchange energy [80, 81]:

$$E_x^{\mathrm{GGA}} = \int d^3r\, n\, \varepsilon_x^{\mathrm{LDA}} F_x(s). \tag{3.12}$$

Although GGA often improves upon the LDA results, e.g. giving more accurate band gaps in semiconductors and bond dissociation energies in molecules, see Fig. 3.2, it famously fails for graphite, where a significant part of the cohesion energy can be contributed to non-local correlations such as van der Waals interactions. Figure 3.3 shows total energies of graphite as a function of the interlayer distance. The calculations were performed with three different approximations to the exchange-correlation functional, i.e. LDA, PBE, and non-local vdW-DF, described in the next section Sec. 3.2.2. The experimental interlayer distance of graphite at ambient conditions is 3.35 Å [77]. By mere chance LDA predicts the correct interlayer distance for this material, while PBE completely fails and while the post-GGA vdW-DF method recovers a minimum at 3.45 Å, which is an overestimation of the interlayer distance by 3%.

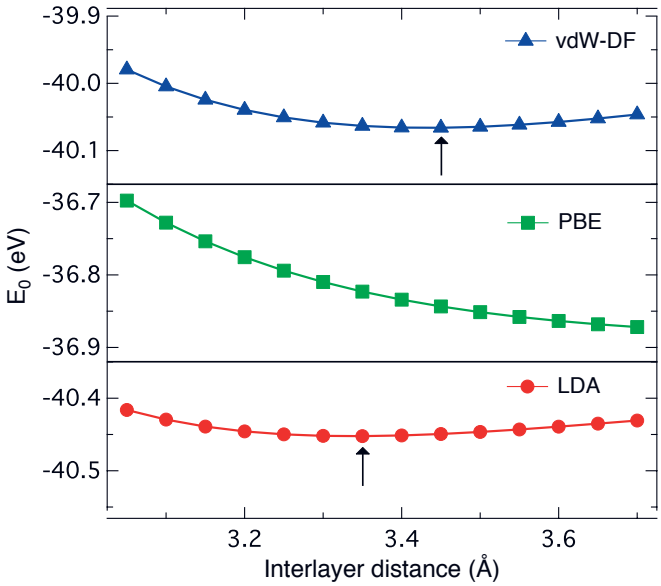

Figure 3.3: Total energy E_0 of graphite versus interlayer distance calculated with three different approximations to the exchange-correlation energy. The arrows mark the minima of the energy curves. Note that the vertical axises show identical energy intervals.

3.2.2 Non-local correlations

J. D. van der Waals studied the gaseous and liquid state of matter in his dissertation, published in 1873, translated and reprinted in Ref. [82]. Starting from the equation of state for an ideal gas, $k_B NT = pV$, he extended this equation to account for the finite size of the molecules and their attractive interaction:

$$N_A k_B T = \left(p + \frac{a}{V^2}\right)(V - b), \tag{3.13}$$

where N_A is the Avogadro constant, k_B the Boltzmann's constant, T the absolute temperature, p the pressure of the fluid, V the volume of the container, a a measure for the attraction between the neutral molecules, and b the volume of the molecules.

Although he postulated an attractive force even between neutral molecules, van der Waals did not have a theory about the force's nature. Today we know that the so-called van der Waals (vdW) forces originate from multipole-multipole, i.e. predominantly dipole-dipole, interactions, whereby one can distinguish between three different scenarios:

1. the interaction of two permanent dipoles [83, 84],
2. the interaction of a permanent dipole and an induced dipole in another molecule [85], and
3. the attraction between two fluctuating dipoles [86, 87].

The interaction energy due to the vdW forces is proportional to the sixth power of the distance between the dipoles. In the following I will concentrate on the third kind of vdW force, which is also known as London dispersion force.

As explained in the previous section, the correct description of material properties within the framework of density functional theory depends essentially on finding an appropriate approximation to the exchange-correlation energy. For dense matter, the (semi-)local approximations are often very successful. But, as we already saw in the case of graphite in Fig. 3.3, these functionals can easily fail for sparse matter that is predominantly hold together by vdW forces. How to treat these dispersion forces with sufficient accuracy is still an active field of research [88].

In the following the theoretical background, i.e. the density functional, to the Jülich Non Local (JuNoLo) code [89], which was used to calculate the vdW contribution to the correlation energy in paper VI, will be presented.

At first, a non-local correlation functional for layered structures was developed [90], which was then generalized to a van der Waals density functional (vdW-DF) for general geometries [91, 92]. In the JuNoLo code this functional is used as a post-processing tool, i.e. it calculates the van der Waals interaction from the charge density that was obtained from an ordinary GGA DFT calculation. It has been shown that the results of this post-processing scheme agree very well with those of a self-consistent implementation [93].

In a first step, one assumes that the new exchange-correlation energy functional ($E_{xc}[n]$) can be written as the sum of the exchange-correlation energy functional from an ordinary DFT calculation (E^0_{xc}[n]) and a non-local correlation functional ($E^{\rm nl}_c[n]$):

$$E_{xc}[n] = E^0_{xc}[n] + E^{\rm nl}_c[n]. \tag{3.14}$$

In the following the derivation of a general functional of the form

$$E^{\rm nl}_c = \frac{1}{2}\int d^3r\, d^3r'\, n(\vec{r})\,\phi(\vec{r},\vec{r}')\,n(\vec{r}') \tag{3.15}$$

will be summarized, see Ref. [91] and the references therein. Here, $\phi(\vec{r},\vec{r}')$ is a general function depending on the difference, $\vec{r}-\vec{r}'$, and the electron densities n in the vicinity of $\vec{r}$ and $\vec{r}'$.

One of the requirements for the functional $E^{\rm nl}_c$ is that the vdW interaction saturates and makes a seamless connection for decreasing distances of the interacting densities.

One starts with the non-local correlation functional, Equ. 25 from Ref. [94],

$$E^{\rm nl}_c = \int_0^\infty \frac{du}{2\pi}{\rm Tr}[\ln(1-V\chi) - \ln\varepsilon], \tag{3.16}$$

where χ is the density response to a fully self-consistent potential, $\delta n = \chi\varphi$. Here, V is the Coulomb interaction, and ε an appropriate approximation of the dielectric function.

From Maxwell's equation

$$\begin{aligned} 4\pi e\delta n &= \nabla\cdot(\vec{E}-\vec{D}) \\ &= \nabla\cdot(1-\varepsilon)\cdot\vec{E} \\ &= \nabla\cdot(\varepsilon-1)\cdot\frac{\nabla\varphi}{e} \end{aligned}$$

it follows that the density response can be written as

$$\chi = (4\pi e^2)^{-1}\nabla\cdot(\varepsilon-1)\cdot\nabla. \tag{3.17}$$

The approximation $E^0_c[n] \approx E^{\rm LDA}_c[n]$ in Equ. (3.14) guarantees the seamlessness of the theory, since for a uniform systems $1-V\chi = \varepsilon$ holds. Hence, the non-local correlation energy, Equ. (3.16), vanishes in this case.

In order to apply Equ. (3.16) to general geometries, it is expanded to second order in $S = 1-\varepsilon^{-1}$:

$$E^{\rm nl}_c \approx \int_0^\infty \frac{du}{4\pi}{\rm Tr}\left[S^2 - \left(\frac{\nabla S\cdot\nabla V}{4\pi e^2}\right)^2\right]. \tag{3.18}$$

Instead of the dielectric function one has now to approximate S. The function S, for convenience written in a plane-wave representation $S_{\vec{q},\vec{q}'}$, has to fulfill the following restrictions:

1. $S_{\vec{q},\vec{q}'}(\omega) \to -\frac{4\pi e^2}{m\omega^2} n_{\vec{q}-\vec{q}'}$ at large frequencies (the f-sum rule, i.e. the charge-current continuity),
2. $\int_{-\infty}^{\infty} S_{\vec{q},\vec{q}'}(iu) \to \frac{8\pi^2 N e^2}{q^2}$ for large q, where N is the number of electrons, to reproduce the exactly known self-correlation,
3. $S_{\vec{q},\vec{q}'} = S_{-\vec{q}',-\vec{q}}$ for time-reversal invariance,
4. a finite $S_{\vec{q},\vec{q}'}(\omega)$ for vanishing q or q' at all nonzero values of ω, to give an exchange-correlation hole with the correct volume (charge conservation).

One can adapt a simple plasmon-pole model for $S_{\vec{q},\vec{q}'} = \frac{1}{2}(\tilde{S}_{\vec{q},\vec{q}'} + \tilde{S}_{-\vec{q}',-\vec{q}})$ as in Ref. [95]:

$$\tilde{S}_{\vec{q},\vec{q}'} = \int d^3r\, e^{-i(\vec{q}-\vec{q}')\cdot\vec{r}} \frac{4\pi\, n(\vec{r})\, e^2}{m(\omega+\omega_q(\vec{r}))(-\omega+\omega_{q'}(\vec{r}))}, \tag{3.19}$$

where the dispersion function $\omega_q(\vec{r})$ depends on the local density and its gradient at $\vec{r}$. The function S will satisfy all four requirements, if one makes the following choice for the dispersion function

$$\omega_q(\vec{r}) = \frac{q^2}{2m} \frac{1}{h(q/q_0(\vec{r}))}, \tag{3.20}$$

with $h(y) = 1 - e^{-\gamma y^2}$, $\gamma = 4\pi/9$, and $q_0^2 = \gamma/l^2$. The dispersion function obeys the limits of $\omega_q = 1/2ml^2$ for small q and of $\omega_q \to q^2/2m$ for large q.

By means of E_{xc}^0 one parametrizes $q_0(\vec{r})$ as a function of the electron density and its gradient at each point. In correspondence to the approximation made in Equ. (3.16), the exchange-correlation functional E_{xc}^0 is given by

$$E_{xc}^0 \approx \int_0^\infty \frac{du}{2\pi} \mathrm{Tr}(\ln\varepsilon) - E_{\mathrm{self}} \approx \int_0^\infty \frac{du}{2\pi} \mathrm{Tr}S - E_{\mathrm{self}}. \tag{3.21}$$

Here, E_{self} is the internal Coulomb self-energy of each electron.

The exchange-correlation energy per electron, $\varepsilon_{xc}^0(\vec{r})$, can be derived by expanding Equ. (3.21) to lowest order in S, substituting it for Equ. (3.19), integrating over $u = -i\omega$, and using $E_{xc}^0 = \int d^3r\, \varepsilon_{xc}^0(\vec{r})\, n(\vec{r})$:

$$\varepsilon_{xc}^0(\vec{r}) = -\frac{3e^2}{4\pi} q_0(\vec{r}). \tag{3.22}$$

With $\varepsilon_x^{\mathrm{LDA}}(\vec{r}) = -3e^2 k_F/4\pi$, $k_F = 3\pi^2 n$ for the homogeneous electron gas, Equ. (3.22) can be rewritten as

$$q_0(\vec{r}) = \frac{\varepsilon_{xc}^0(\vec{r})}{\varepsilon_x^{\mathrm{LDA}}(\vec{r})} k_F(\vec{r}). \tag{3.23}$$

The approximation used for $\varepsilon_{xc}^0(\vec{r})$ is the so-called LDA with gradient corrections, i.e.

$$\varepsilon_{xc}^0 \approx \varepsilon_{xc}^{\mathrm{LDA}} - \varepsilon_x^{\mathrm{LDA}} \left[-\frac{0.8491}{9} \left(\frac{\nabla n}{2k_F n} \right)^2 \right], \tag{3.24}$$

which finally allows to calculate the dispersion function and hence Equ. (3.18). This equation reads in plane-wave representation

$$E_{xc}^{\mathrm{nl}} = \int_0^\infty \frac{du}{4\pi} \sum_{\vec{q},\vec{q}'} (1 - (\hat{q}\cdot\hat{q}')^2) S_{\vec{q},\vec{q}'} S_{\vec{q}',\vec{q}}, \tag{3.25}$$

which can be brought into the desired form of Equ. (3.16) with the kernel

$$\phi(\vec{r},\vec{r}') = \frac{2me^4}{\pi^2} \int_0^\infty a^2 da \int_0^\infty b^2 db\, W(a,b)\, T(\nu(a),\nu(b),\nu'(a),\nu'(b)), \tag{3.26}$$

where

$$T(w,x,y,z) = \frac{1}{2} \left(\frac{1}{w+x} + \frac{1}{y+z} \right) \left(\frac{1}{(w+y)(x+z)} + \frac{1}{(w+z)(y+x)} \right) \tag{3.27}$$

and

$$\begin{aligned} W(a,b) &= \frac{2}{a^3 b^3} [(3-a^2) b \cos b \sin a + (3-b^2) a \cos a \sin b & (3.28)\\ &+ (a^2+b^2-3) \sin a \sin b - 3ab \cos a \cos b]. & (3.29) \end{aligned}$$

Here, ν and ν' are given by $\nu(y) = y^2/2h(y/d)$ and $\nu'(y) = y^2/2h(y/d')$ with $d = |\vec{r}-\vec{r}'|q_0(\vec{r})$ and $d' = |\vec{r}-\vec{r}'|q_0(\vec{r}')$.

So the kernel ϕ in Equ. (3.15) only depends on $\vec{r}$ and $\vec{r}'$ and thus can be tabulated in advance in terms of $0 \le D < \infty$ and $0 \le \delta < 1$, i.e. $d = D(1+\delta)$ and $d' = D(1-\delta)$.

As desired, the kernel recovers the $1/R^6$ behavior of the van der Waals force

$$\phi \to -\frac{C}{d^2 d'^2 (d^2 + d'^2)} \tag{3.30}$$

for large distances d and d'.

Before moving on to the description of the DFT implementation used for most of the calculations in papers I-VI, it shall be mentioned that there exists a number of semi-empirical methods to include vdW interactions in DFT calculations [96–99]. Also, there are alternative approaches as well, more in the spirit of Jacob's ladder [74], that employ exact-exchange and the random phase approximation [100]. Recent studies of adsorbed aromatic molecules on coinage metal surfaces have shown that all mentioned descriptions of vdW interactions produce fairly similar results for these kind of systems [100–103]. For graphite, on the other hand, the different methods disagree more substantially [104]. For cases tested so far, none of the methods showed a decisive advantage in terms of correctly predicting adsorption energies, bond length, and being computationally efficient.

4. VASP - our implementation of choice

4.1 The Projector Augmented-Wave method

P. E. Blöchl introduced the projector augmented-wave (PAW) method [105] as a natural extension of the linear augmented-wave method [106] and the norm-conserving pseudopotential method [107] to solve the Kohn-Sham problem Equ. (3.9) for the auxiliary system of non-interacting particles in an effective potential.

The difficulties to calculate the electronic structures of real materials arise from the fact that the potential $V_{\mathrm{KS}}^{\sigma}(\vec{r})$, Equ. (3.8), varies greatly in different spatial regions, e.g. around the nuclei and in the bonding regions. Hence also the wave function has very different properties in these different regions. The practical challenge lies in describing the bonding with a high accuracy and at the same time accounting for the rapid oscillations around the nuclei. The basic idea behind the projector augmented-wave method is to find a linear transformation $\mathscr{T}$ for the all-electron (AE) Kohn-Sham wave function in Equ. (3.9), which gives computationally convenient pseudo (PS) wave functions. One assumes that the transformation is of the form

$$\mathscr{T} = 1 + \sum_R \mathscr{T}_R, \tag{4.1}$$

i.e. it only differs from unity by local contributions $\mathscr{T}_R$ that act within some augmentation region, Ω_R, around an atom at position R. The local transformations, $\mathscr{T}_R$, are defined within Ω_R as

$$|\phi_i\rangle = (1 + \mathscr{T}_R)\,|\tilde{\phi}_i\rangle\,, \tag{4.2}$$

where $|\phi_i\rangle$ are AE partial waves, e.g. solutions to the radial Schrödinger equation for the atom species one is interested in, and $|\tilde{\phi}_i\rangle$ are PS partial waves that are orthogonal to the core states and complete in the augmentation region Ω_R. The indices i include both the atomic site R and the angular momentum quantum numbers $L = (l,m)$. Note that by construction of the linear transformation, Equ. (4.1), $|\tilde{\phi}_i\rangle$ and $|\phi_i\rangle$ are identical outside Ω_R.

Within Ω_R, every PS wave function can be written as a sum of PS partial waves

$$|\tilde{\Psi}\rangle = \sum_i c_i \, |\tilde{\phi}_i\rangle \,. \tag{4.3}$$

Since $|\phi\rangle = \mathscr{T} \, |\tilde{\phi}_i\rangle$, it follows that

$$|\Psi\rangle = \mathscr{T} \, |\tilde{\Psi}\rangle = \sum_i c_i \, |\phi_i\rangle \tag{4.4}$$

and

$$|\Psi\rangle = |\tilde{\Psi}\rangle - \sum_i c_i \, |\tilde{\phi}_i\rangle + \sum_i c_i \, |\phi_i\rangle \,. \tag{4.5}$$

Due to the required linearity of $\mathscr{T}$, the coefficients c_i have to be linear functionals of $|\tilde{\Psi}\rangle$, i.e.

$$c_i = \langle \tilde{p}_i | \tilde{\Psi} \rangle \,, \tag{4.6}$$

with some fixed projector functions $|\tilde{p}_i\rangle$ for each $|\tilde{\phi}_i\rangle$. From the requirement $\sum_i |\tilde{\phi}_i\rangle \langle \tilde{p}_i| = 1$ in Ω_R, it follows that $\langle \tilde{p}_i | \tilde{\phi}_j \rangle = \delta_{ij}$.

Thus, in summary the AE wave function can be determined by

$$|\Psi\rangle = |\tilde{\Psi}\rangle + \sum_i (|\phi_i\rangle - |\tilde{\phi}_i\rangle) \, \langle \tilde{p}_i | \tilde{\Psi} \rangle \,. \tag{4.7}$$

Similarly, the core states, $|\Psi^c\rangle$, can be decomposed as

$$|\Psi^c\rangle = |\tilde{\Psi}^c\rangle + |\phi^c\rangle - |\tilde{\phi}^c\rangle \,. \tag{4.8}$$

Note that the frozen-core-approximation is applied here, i.e. $|\Psi^c\rangle$ is taken from the core states of isolated atoms.

As usual, the expectation values of an operator A, e.g. the density or total energy, is given by

$$\langle A \rangle = \sum_n f_n \, \langle \Psi_n | A | \Psi_n \rangle = \sum_n f_n \, \langle \tilde{\Psi}_n | \tilde{A} | \tilde{\Psi}_n \rangle \,, \tag{4.9}$$

with

$$\begin{aligned} \tilde{A} &= \mathscr{T}^\dagger A \mathscr{T} \\ &= A + \sum_{i,j} |\tilde{p}_i\rangle \, (\langle \phi_i | A | \phi_j \rangle - \langle \tilde{\phi}_i | A | \tilde{\phi}_j \rangle) \, \langle \tilde{p}_i | \,, \end{aligned} \tag{4.10}$$

where n is the band index, and f_n the occupation of the state.

Except for the frozen-core approximation and a parametrization of the exchange-correlation functional, the presented PAW method is an exact implementation of the density functional theory. In practice, one has to choose a basis set for $|\tilde{\Psi}\rangle$, $|\phi_i\rangle$, and $|\tilde{\phi}_i\rangle$. This requires certain approximations to limit the number of basis wave functions, e.g. a cut-off energy and a maximum angular quantum number, which have to be appropriately chosen to fulfill the desired convergence criterium.

The DFT implementation used for the calculations in papers I - VI was the Vienna Ab-Initio Simulation package (VASP) [108–110].[1] It allows to perform *ab-initio* quantum-mechanical molecular dynamics simulations employing pseudopotentials, a plane wave basis set, and the PAW method.

4.2 Equilibrium

One of the oldest problems in solid state physics, that was tackled by density functional theory, is the calculation of equilibrium crystal structures. For simple structures this can easily be achieved by calculating the total energies for a series of lattice parameters in order to find the ground state structure. But most crystalline materials, e.g. those containing more than two atomic species, have a number of internal parameters, which makes it cumbersome to manually determine their equilibrium structure. Two classes of methods to find the minimum of the Kohn-Sham total energy with respect to a structural optimization exist. The first class comprises Monte-Carlo methods to minimize the Kohn-Sham energy by simulated annealing, first developed by Car and Parrinello [111]. The second class are self-consistent cycle methods, where the Hellmann-Feynman theorem, Refs [112–114],

$$\frac{\partial E}{\partial \lambda} = \int \psi^*(\lambda)\, \frac{\partial H_\lambda}{\partial \lambda}\, \psi(\lambda)\, d\tau \tag{4.11}$$

is used to calculate the forces that act on the nuclei at position R,

$$F_R = -\frac{\partial E_{\mathrm{KS}}}{\partial R}\Big|_{|\tilde{\Psi}\rangle}. \tag{4.12}$$

In Equ. (4.11) H_λ is the hamiltonian of the considered system, which depends on continuous parameters λ, e.g. the coordinates of the nuclei, $\psi(\lambda)$ is the corresponding wave function, E is the energy of the system, and $d\tau$ means an integration over the whole domain of the wave function. The Hellmann-Feynman forces, Equ. (4.12) are minimized for the considered system in order to find its equilibrium structure, i.e. the

[1] In paper IV also the Gaussian09 program package was used to calculate e. g. the vibrational frequencies.

geometry where the forces vanish. Those self-consistent cycle methods can be build upon the PAW method [105] in a straight forward way, i.e. as shown in Equ. (4.12) as a partial derivative of the KS total energy with respect to the atomic positions, where the variational parameters of the PS wave function are kept fixed.

With this, we close the first part of this Thesis that gave an introduction into the historical development of condensed matter theory and the used methodology. In the following Chapter 5 the results of papers I - VI will be summarized.

5. A summary of papers I - VI

During the last two years of my PhD studies, I researched a number of different systems from the fields of surface science and cluster physics, using density functional theory (DFT) calculations.

In the first set of projects, papers I - IV (Section 5.2), we addressed properties of small gold clusters. The smallest possible gold clusters, consisting of one to four atoms only, supported on a regular (001) magnesium oxide terrace were the first systems to be investigated.

By studying the (co-)adsorption of carbon monoxide and oxygen on these systems, I was able to explain the absence ($Au_{1,2}$), respective low ($Au_{3,4}$) catalytic activities that have been observed in experiments [115] (paper I).

Inspired by the theoretical prediction of a water mediated CO oxidation reaction on Au_8/MgO [116], I studied this reaction pathway for Au_{1-4}/MgO in paper II. I found that this reaction pathway is not accessible for $Au_{2,4}$/MgO and very unlikely in the case of $Au_{1,3}$/MgO.

The number thirteen, otherwise rather related to bad fortune in our culture, is considered to be one of the 'magic' numbers, when it comes to the number of atoms contained in metal clusters [117,118]. I studied the structural stability of Au_{13} isomers with respect to the inclusion of spin-orbit coupling and the potential of Au_{13} for oxygen dissociation (paper III).

Paper IV addresses a more fundamental aspect of small coinage metal clusters that has been widely neglected so far: thermal vibration modes. I performed thorough scans of the Born-Oppenheimer potential energy surface for copper, silver, and gold trimers, both charged and neutral, to estimate which structures are thermally accessiblea lready at room temperature. By means of linear response theory, we calculated thermally excited vibration modes and, taking Au_3 as a showcase, I studied the influence of these modes on the binding of carbon monoxide on the cluster.

After its successful synthesis [119–121], graphene, the two-dimensional building block of graphite, gained much attention in recent years, because of its unique electronic properties [122–124].[1] In recent experiments, it was observed that gold forms nanometer-sized clusters on graphene [125], even when it is deposited as single atoms. In paper V (Section 5.3), I studied the mobility and the clustering mechanism of Au_{1-4} on graphene.

[1]The attention even reached into the mass-media for one or two days, when the Nobel Prize in Physics 2010 was awarded jointly to Andre Geim and Konstantin Novoselov 'for groundbreaking experiments regarding the two-dimensional material graphene.'

Graphite is a classical example of a material that is held together by van der Waals forces [99]. Those non-local interactions might even play a role in correctly describing the cohesive properties of coinage metals in bulk [126]. Therefore, it is only natural to ask what role van der Waals forces play for the adsorption of Cu, Ag, and Au on graphene. We address this issue in paper VI (Section 5.3). Therein we show that silver is purely physisorbed on graphene, while the binding of copper and gold to graphene is a mixture of chemical binding and van der Waals forces.

Before moving on to the results, the most relevant computational details for all my calculations are summarized in the following section.

5.1 Computational details

Plane wave related methods, such as the projector augmented-wave method (PAW) [105], were originally developed to calculate bulk materials, i.e. systems that are periodic in all three dimensions. Nonetheless, these methods are also suitable for calculating surfaces, interfaces, clusters, and molecules, if one uses the so-called supercell approach. To do so, one artificially creates a periodicity in those dimensions where the system is not periodic in itself. For example, surfaces are treated as stacks of two-dimensional slabs, that consist of a few atom layers. These slabs have to be well-separated from each other by a thick layer of vacuum to suppress their mutual interaction.

The MgO(001) bulk surface in papers I and II was modeled in a super-cell approach with a two monolayer thick 3×3 MgO slab. The unit cell was constructed using the equilibrium lattice parameter of MgO (4.235 Å) obtained in the corresponding bulk calculations. The repeated slabs were separated from each other by 27 Å of vacuum.

The graphene sheet in papers V and VI was modeled by a 5×5 supercell, i.e. 50 carbon atoms, using the calculated C-C bond length of 1.42 Å. The repeated images of the sheet were separated by 20 Å of vacuum.

The images of molecules and clusters in the gas phase were separated by at least 15 Å of vacuum.

All my scalar-relativistic *ab-initio* DFT calculations were performed using the PAW method [105, 110] as implemented in VASP [108–110]. As mentioned in Section 3.2.1, the exchange-correlation interaction was treated in the generalized gradient approximation (GGA) in the parameterization of Perdew, Burke, and Ernzerhof (PBE) [80] (papers I - VI). In the method section of paper IV, we show that the properties of coinage metal dimer calculated in PBE do favorably compare to the results obtained with a number of higher-level methods, making PBE an adequate approximation.

In paper VI the local density approximation (LDA) in the parametrization of Perdew and Zunger [127] was used for comparison, too.

In the same paper VI, we also accounted for non-local correlation energies by employing two different methods: the van der Waals density functional (vdW-DF) method [90–92] as implemented in the Jülich Non-Local (JuNoLo) code [89] (see Section 3.2.2 for more details) and the density functional theory plus long-range dispersion correction (DFT+D2) method [98] in the implementation of Ref. [99]. Both methods differ from each other in various aspects. While vdW-DF is an *ab-initio* post-processing method, that does not allow for relaxations in the JuNoLo implementation, the employed DFT+D2 implementation allows to include the vdW interactions in the self-consistency cycle, i.e. during structural relaxations. The DFT+D2 method is relatively computationally inexpensive compared to JuNoLo, since the vdW interactions are described by a pair-wise correction, which is optimized for some popular DFT functionals, and added to the self-consistent Kohn-Sham energy.

Throughout the projects, a Monkhorst-Pack Γ-centered k-point mesh was used for the structural relaxations. The grid was adapted to the individual studies to ensure convergence of the physical quantities in question. For instance, in paper V, the geometrical structures of Au_{1-4}/graphene are sufficiently well relaxed with a $5 \times 5 \times 1$ k-point mesh (13 k-points in the irreducible wedge of the Brillouin-Zone), while at least a $16 \times 16 \times 1$ k-point mesh is necessary to accurately calculate the density of states (DOS) of these systems. For atoms, molecules, and clusters in the gas phase only the Γ-point needs to be evaluated.

To obtain the ground state structures, the relaxation cycle was stopped when the Hellmann-Feynman forces, see Section 4.2, had become smaller than $5 \cdot 10^{-3}$ eV/Å on the atoms that were free to relax.

The cut-off energy of the plane waves as well as the width of the Gaussian smearing for the occupation of the electronic levels had to be adapted to the individual problem to ensure the convergence of the total energy.

In all calculations, I took spin-polarization into account. Additionally, spin-orbit coupling (SOC) was only included in papers I, III, and IV.

The adsorption energy (E_{ads}) of molecules and clusters (M) on, for instance, a surface (S) are calculated as

$$E_{\mathrm{ads}} = E_0[\mathrm{M/S}] - E_0[\mathrm{S}] - E_0[\mathrm{M}], \tag{5.1}$$

where $E_0[\mathrm{M/S}]$ is the energy of the molecule adsorbed on the substrate, $E_0[\mathrm{S}]$ is the energy of the undistorted substrate, and $E_0[\mathrm{M}]$ is the ground state energy of the molecule in the gas phase. Note that the E_{ads} are negative when the adsorption is exothermic.

The charge distributions and transfers were analyzed by means of the Bader analysis [128]. The figures, illustrating atomic structures and charge

density redistributions, were created with the Visualization for Electronic and Structural Analysis (VESTA) program.

5.2 Nanocatalysis by gold

Man used catalytic reactions, e.g. the alcoholic fermentation, for thousands of years without any deeper understanding of the underlying chemical processes. Although, the term catalysis was introduced by J. J. Berzelius, 'den svenska kemins fader' (the father of chemistry in Sweden), in 1835 [129], six more decades had to pass before a kinetic definition of catalysis was formulated by W. Ostwald [130].[2]

In nanoscience, one studies the manipulation and control of matter on an atomic scale.[3] Nanocatalysis can be classified as a subfield of nanoscience. Unlike ordinary 'macroscopic' catalytic materials, the performance of nanocatalysts does not simply scale, for instance, with the surface to volume ratio of the active material. U. Heiz and U. Landman defined, from Ref. [132]: 'The central aim of nanocatalysis is the promotion, enhancement, steering and control of chemical reactions by changing the size, dimensionality, chemical composition, morphology, or charge state of the catalyst or the reaction center, and/or by changing the kinetics through nanopattering of the catalytic reaction centers. Since the aforementioned size-dependent non-scaleable, and often non-monotonic, evolution of materials' properties may occur when at least one of the material's dimensions is reduced to the nanoscale, nanocatalytic systems may appear as ultra-thin films, nanowires, or clusters. For these systems the chemical and physical properties are often controlled by quantum size effects and they present new opportunities for an atom-by-atom design, tuning and control of chemical activity, specificity, and selectivity.'[4]

Gold was among the first metals to be used by man.[5] Although chemically inert in bulk, minuscule gold particles can be catalytically active. This property has received much attention since Haruta showed that supported nanometer-sized gold particles have a substantial catalytic activity towards

[2]Ostwald refined his definition over the years. In general, one can define catalysis as the change in rate of a chemical reaction due to the participation of a so-called catalyst, i.e. an additional substance, which is not consumed in the reaction.

[3]C. Joachim, a pioneer in this field, published a popular science book on the rise and the future opportunities of nanoscience [131], which is a compelling introduction.

[4]Therefore the chosen subheading of this Thesis.

[5]Gold's physical and chemical properties, i.e. color, density, resistance to corrosion, a melting temperature close to copper's, as well as its scarcity, made it a precious commodity from the early civilizations until today. The convertibility of national currencies to gold, which had been first introduced by Sir I. Newton as Master of the Mint in Britain in 1707, was not terminated before the breakdown of the Bretton Woods system in 1973. Nonetheless, national banks and international organizations still store roughly $9.336 \cdot 10^{31}$ gold atoms in their vaults.

low-temperature oxidation of carbon monoxide [133] . However, already in 1823, J. W. Döbereiner [134] in Jena as well as P. L. Dulong and L. G. Thenard [135] found that gold is among the metals that catalyze the decomposition of ammonia, as pointed out in Ref. [136].[6]

Gold clusters can be used for homogeneous as well as heterogeneous catalysis and there exists a number of review articles on the engineering, experimental, and theoretical aspects of the subject, for instance Refs [137–140]. Especially, Pyykkö's extensive reviews on the theoretical chemistry of gold are recommended, as they contain an extensive collection of references [141–143].

5.2.1 Au_{1-4} on bulk MgO and CO oxidation

Small gold clusters in the gas phase, containing less than 100 atoms, have been the subject of much research. Spectroscopic measurements on small gold clusters date already back to the early 1980s [144–147]. The ground state structures and electronic properties of these small gold clusters, charged and neutral, have also been extensively studied by means of density functional theory [148–157]. Since the importance of relativistic effects on the properties of gold are well-known [158], the impact of spin-orbit coupling on the structures and electronic properties of small gold clusters has been widely studied by theory as well [159–161].

The oxidation of carbon monoxide on gold clusters is among the most studied reactions in this field. Anionic gold clusters as small as dimers have been shown, by experiment and theory, to be catalytic active towards CO oxidation in the gas phase [162–164]. Gold clusters have been deposited on a range of metal-oxide supports, e.g. Haruta used in his original studies Fe_2O_3, Co_3O_4, and NiO [133]. From a theoretical point of view, bulk surfaces of TiO_2 [165, 166] and MgO [115, 167–169] are probably the most widely studied ones.

In paper I, we explain the experimentally found catalytic characteristics of Au_{1-4}/MgO(100) towards CO oxidation, cf. Ref. [115], by means of a comprehensive density functional study of their ability to (co-)adsorb CO and O_2 molecules.

First, we determine the ground state structures of Au_{1-4}/MgO(100), see Fig. 5.1 for an illustration, and analyze the binding mechanism of Au to the surface oxygen, the influence of spin-orbit coupling in the adsorption energies and the charge transfer from the substrate into the clusters, see Fig. 5.2.

In panel (a) of Fig. 5.2 the calculated adsorption energies, with SOC taken into account, are shown. They range from -0.89 (Au_1) to -1.75 eV (Au_4).

[6]This historical example should remind the reader to always strive for a swift publication of results: Dulong and Thenard received word of Döbereiner's work, reproduced it in their laboratory, and managed to publish it before him.

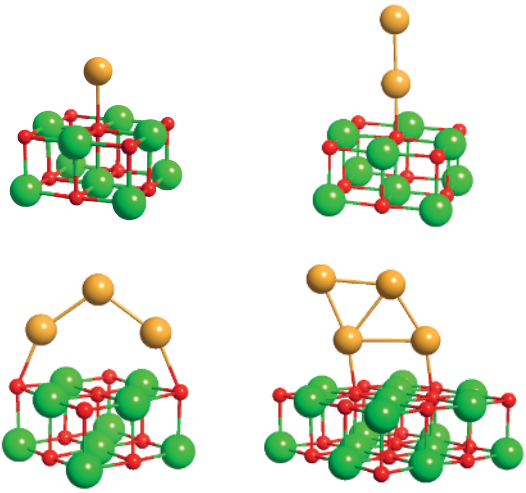

Figure 5.1: An illustration of the ground state structures of Au_{1-4}/MgO(100). The different atom species are illustrated as yellow (Au), red (O), and green (Mg) balls, respectively. The chemical bonds between the atoms are shown as (bi-)colored sticks. Note that only a part of the actually substrate is shown.

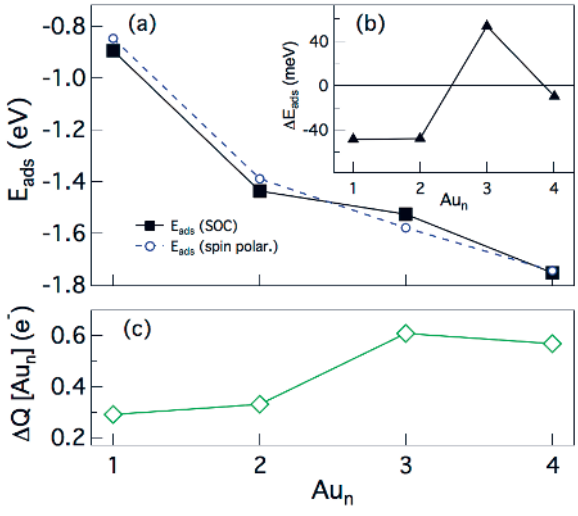

Figure 5.2: Panel (a): adsorption energies E_{ads} of Au_{1-4} on a regular MgO(100) terrace. For comparison the results of calculations with spin-orbit coupling (SOC) taken into account (solid squares) and those without, i.e. spin polarized only (sp), (open circles) are shown. Inset (b): effect of SOC on the adsorption energies, $\Delta E_{ads} = E_{ads}^{SOC} - E_{ads}^{sp}$. Lower panel (c): total Bader charge transfered from the MgO substrate into the adsorbed Au_{1-4}.

Including SOC changes the adsorption energies by less than 5% compared to spin polarized calculations, as can be seen from the inset (b) in Fig. 5.2. In panel (c) of the same figure, the charge donation from the surface oxygen atoms into the clusters is shown. It scales linearly with approximately 0.3 e^- per Au-O bond. Since the clusters $Au_{1,3}$ have an unpaired electron, they also induce a spin moment into the underlying oxygen atoms of the substrate.

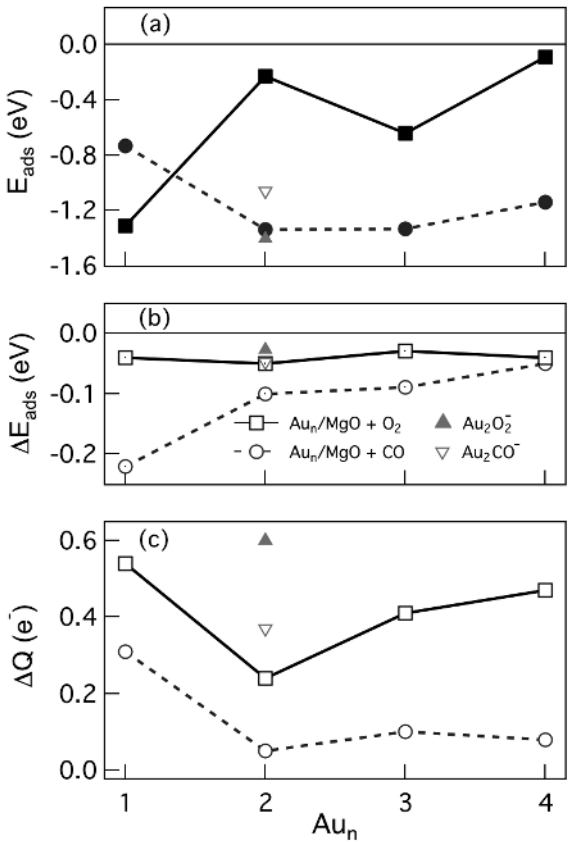

Figure 5.3: CO and O_2 adsorbed on Au_{1-4}/MgO, their adsorption energies and charge transfers. Upper panel (a): E_{ads} of CO (circles) and O_2 (squares). For comparison, the binding energies of CO (open triangle) and O_2 (solid triangle) on Au_2^- in the gas phase are also shown. Middle panel (b): impact of the inclusion of SOC on the E_{ads}, cf. Fig. 5.2. Lower panel (c): charge transfer ΔQ to CO (circles) and O_2 (squares) from Au_{1-4}/MgO. Note that in the case of Au_2CO/O_2^- (open and solid triangle, respectively) the available extra charge is one electron, compared to a maximum of 0.61 e^- in the case of Au_4/MgO, therefore the significantly higher charge transfer for the system in the gas phase.

In a subsequent step, we systematically study the adsorption of a CO and an O_2 molecule on the ground state structures of Au_{1-4}/MgO(100). Panel (a) of Fig. 5.3 shows the adsorption energies of CO and O_2 on Au_{1-4}/MgO.

Oxygen binds strongest to Au_1/MgO and its adsorption energy oscillates with the parity of the gold clusters. Carbon monoxide, on the other hand, does not show these oscillations and binds significantly stronger than oxygen to the bigger clusters, Au_{2-4}/MgO. For comparison also the binding energies of CO and O_2 to the anionic dimer in the gas phase are shown in Fig. 5.3 (a).

In Fig. 5.3 (b) the influence of SOC on the adsorption energies of CO and O_2 is shown, i.e. $\Delta E_{\mathrm{ads}} = E_{\mathrm{ads}}^{\mathrm{SOC}} - E_{\mathrm{ads}}^{\mathrm{sp}}$. Here $E_{\mathrm{ads}}^{\mathrm{SOC}}$ ($E_{\mathrm{ads}}^{\mathrm{sp}}$) are the adsorption energies with (without) taking SOC into account. The effect is most significant for CO on Au_1/MgO, i.e. ΔE_{ads} = -0.21 eV. As in the case of Au_{1-4}/MgO, see Fig. 5.2, the influence of SOC on the adsorption energies decreases quickly with increasing cluster size.

Finally, the lower panel (c) in Fig. 5.3 shows the additional charge on CO and O_2, that the molecules receive from the cluster/substrate system. Due to the much higher electron affinity of O_2 (1.16 eV) compared to that of CO (0.29 eV) more charge is transferred from Au_{1-4}/MgO to O_2 than to CO.

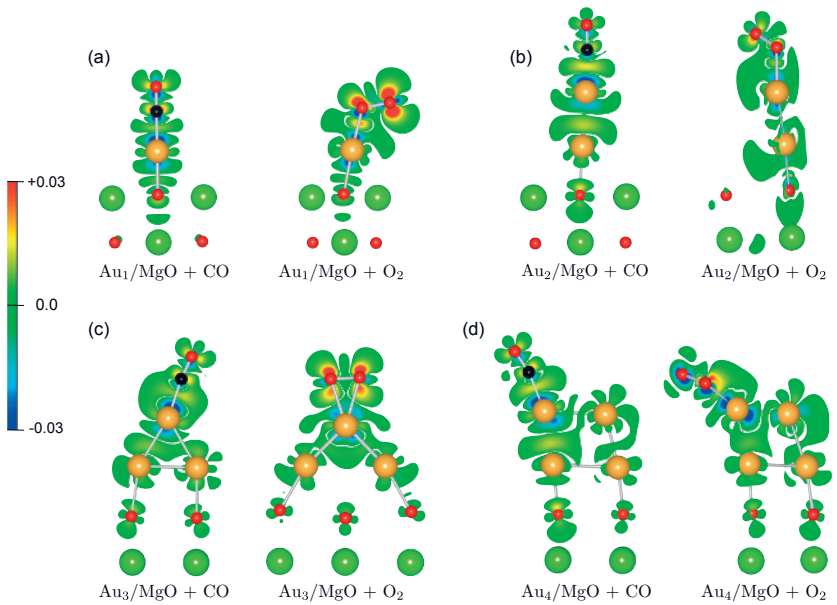

Figure 5.4: The ground state geometries of Au_{1-4}/MgO + CO (O_2). The different atom species are illustrated as yellow (Au), red (O), black (C), and green (Mg) balls, respectively. Also shown are cuts through the charge density redistribution $\Delta\rho$ = ρ[Au_n/MgO + CO/O_2] - ρ[Au_n] - ρ[MgO] - ρ[CO/O_2] along different planes.

In order to gain more insight into the binding mechanism of the molecules to the clusters, the charge density redistribution upon adsorption of the molecules is presented in Fig. 5.4. A substantial fraction of the additional charge, assigned by the Bader analysis to CO, is actually located in between Au and C, cf. 5.4, indicating the formation of a covalent bond. Furthermore, an intramolecular charge redistribution from oxygen towards

carbon can be seen in the CO molecule. In the case of adsorbed O_2 most of the additional charge from the cluster is donated further into the molecule, i.e. the extra charge tends to be concentrated as far away from the gold cluster as possible, see Fig. 5.4.

In conclusion, we expect from the calculated adsorption energies the following ground state structures under mixed atmosphere of CO and O_2: Au_1O_2/MgO and Au_{2-4}CO/MgO.

The anionic gold dimer in the gas phase has been shown to exhibit a considerable catalytic activity. [162, 164] In particular, the following Eley-Rideal reaction mechanism for the CO oxidation with Au_2^- as a catalyst has been suggested, Ref. [164]:

$$\begin{aligned} Au_2^- + O_2 &\rightarrow Au_2O_2^- \\ Au_2O_2^- + CO &\rightleftharpoons Au_2(CO)O_2^- \\ Au_2(CO)O_2^- + CO &\rightarrow Au_2^- + 2CO_2 \end{aligned}$$

For supported gold clusters a Langmuir-Hinshelwood reaction scheme, where adsorbents can thermalize and long-lived transition species exist, would be expected instead.

As mentioned at the beginning of this section, $Au_{1,2}$/MgO were experimentally found to be catalytically inactive under such a mixed CO/O_2 atmosphere [115]. This could be explained by our following results: First, we find it impossible to co-adsorb CO on Au_1O_2/MgO, i.e. to form a carbonate-like (CO_3) transition state, which should exist as an intermediate state during an oxidation reaction.

For the supported dimer, on the other hand, such a carbonate-like transition state could be formed from Au_2O_2/MgO and CO. Even a catalytic reaction cycle towards CO oxidation, analogous to the gas phase reaction involving Au_2^-, is energetically possible for Au_2/MgO. But, as stated above, under a mixed atmosphere, we expect the gold dimer to be blocked by CO. Starting from Au_2CO/MgO, it is not possible to co-adsorb O_2 and hence the proposed catalytic cycle can not be found.

Although a carbonate-like state could not be formed on $Au_{3,4}$/MgO either, it appears to be possible to co-adsorb CO and O_2 at different sites of these clusters. This indicates that a Langmuir-Hinshelwood reaction mechanism could occur in these systems, which would explain the catalytic activity of these clusters taht has been observed experimentally [115].

The subsequent paper II is in some respects a continuation of paper I. In Ref. [116] a water mediated CO oxidation cycle has been proposed for the eight atom gold cluster on a regular MgO terrace. In paper II, we address the question, whether the presence of H_2O influences the catalytic activity of Au_{1-4}/MgO towards the oxidation of carbon monoxide.

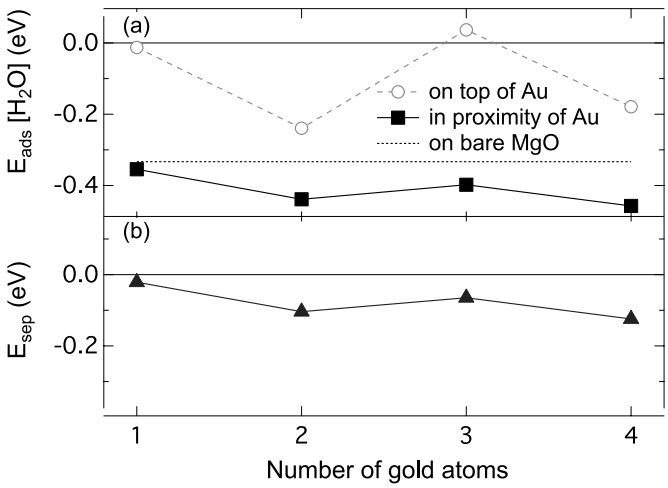

Figure 5.5: Top panel (a): Adsorption energies of H_2O in the proximity (solid squares) and on top of Au_{1-4}/MgO (open circles). The dashed horizontal line shows E_{ads} of H_2O on bare MgO. Lower panel (b): the separation energy $E_{sep} = E_0[Au_n/MgO$ with H_2O in proximity] - $E_0[Au_n/MgO]$ - $E_0[H_2O/MgO]$ (solid triangles). Note that these points coincide with the solid squares in panel (a), i.e. E_{ads} $[Au_{1-4}]$ is not affected by the proximity of H_2O.

To this end, we study the (co-)adsorption of H_2O and CO/O_2 on these small gold clusters. At first, we calculate the adsorption of H_2O and find two sets of stable adsorption sites for H_2O: in the proximity and on top of Au_{1-4}/MgO, see Fig. 5.5 (a). We find that adsorbing the water molecule on the second-nearest magnesium atom from the gold cluster is energetically the most favorable site.

From calculating the adsorption energies of H_2O on pre-adsorbed CO and O_2 on Au_{1-4}/MgO we find the following ground state structures in the presence of all three molecular species: Au_1O_2/MgO and $Au_{2-4}CO$/MgO with H_2O adsorbed on the surface in the proximity of the clusters-molecule complex, see Fig. 5.6 for an illustration of all structures with H_2O in the proximity. In these configurations the adsorption energies of CO and O_2 are not significantly changed compared to the water free scenario studied in paper I, see Fig. 5.3. Also, the catalytic activity of Au_{1-4}/MgO is indifferent to the presence of H_2O in the proximity of the cluster/molecule complex.

Nonetheless, as in case of Au_8/MgO, Ref. [116], we find that an oxygen and a water molecule can form a stable, highly activated

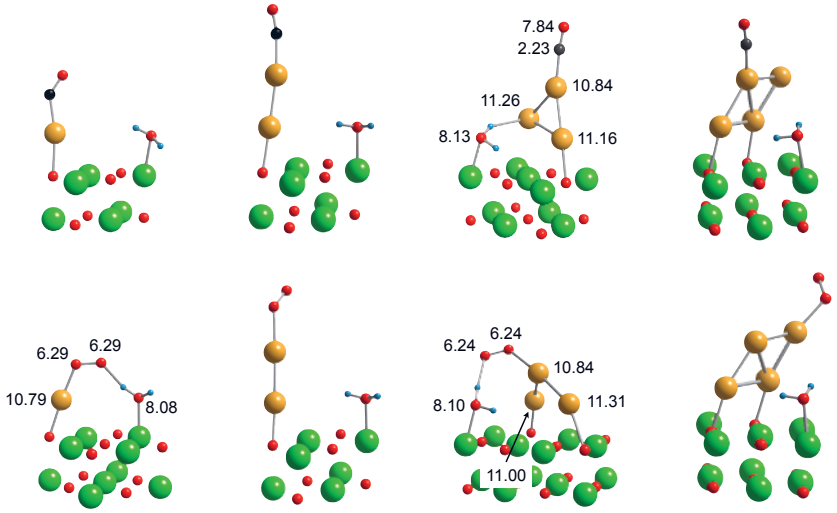

Figure 5.6: Ground state structures of CO/O_2 and H_2O co-adsorbed on Au_{1-4}/MgO. In the three cases were new bonds are formed also the Bader charges are shown (in e^-). In the gas phase carbon monoxide has Bader charges of 2.25 (C) and 7.75 (O) and the oxygen molecule of 6 per O-atom. The different atom species are illustrated as yellow (Au), red (O), black (C), green (Mg), and blue (H) balls, respectively.

hydroperoxyl-hydroxyl ($O_2H\cdots OH$) complex on $Au_{1,3}/MgO$. But in contrast to Au_8/MgO, these complexes are unlikely to open a water mediated catalytic reaction pathway towards CO oxidation, see Figs 5.7 and 5.8.

In both cases, i.e. $Au_{1,3}/MgO$, the formation of the first CO_2 molecule from a CO molecule and an oxygen atom from the hydroperoxyl group involves an activation barrier. From a restricted molecular dynamics simulation, we obtain activation energies for this oxidation reaction of 0.5 eV for Au_1 and 0.6 eV for Au_3, respectively. Clearly, the kinetic energy of the CO molecule has to exceed these activation energies to overcome the barrier. Thus, a necessary condition for the oxidation reaction to happen is that the strength of the bonds B2 - B4 in the molecular complex, shown in the insets of Figs 5.7 and 5.8, exceeds the kinetic energy of CO. This might occur for Au_1/MgO, since the remaining bonds B2 - B4 in the $O_2H\cdots OH$ complex have bond dissociation energies of at least 1.27 eV. However, the remaining complex $(OH)_2$ on Au_1/MgO undergoes a barrier free dissociation into two hydroxyl groups. One of which is adsorbed on the adatom and the other one nearby on the MgO surface. This dissociation is possible since bond B3 is weakened to 0.6 eV once the oxygen atom is removed from the hydroperoxyl group. On MgO, on the other hand, the adsorption energy of an OH group is -1.19 eV, making this site energetically more favorable for OH. Since both OH groups are inert towards a reaction with a CO molecule the catalytic cycle is interrupted.

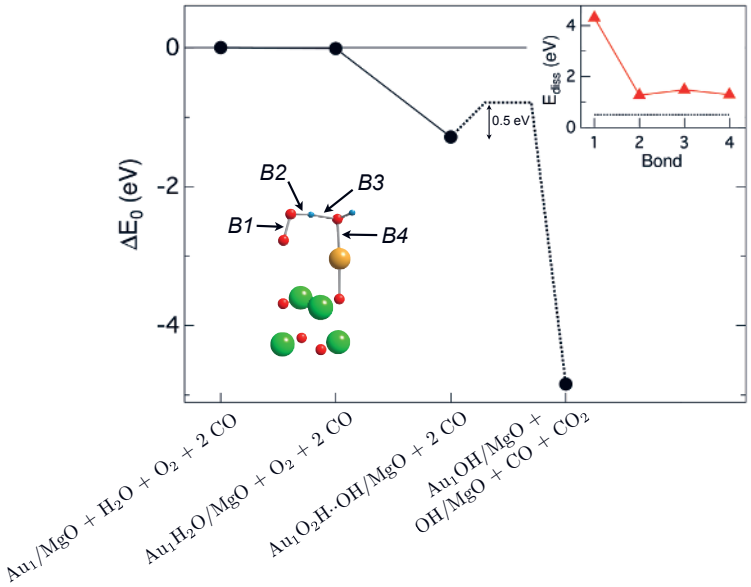

Figure 5.7: Change in the total energy during the successive adsorption of H_2O, O_2, and CO on Au_1/MgO. After the formation of a CO_2 the remaining complex break apart into two OH groups, one on the adatom and one on the surface nearby. The upper-right inset shows the bond dissociation energies of B1 - B4 (solid triangles) compared to the activation barrier (dotted line) of the $O_2H\cdots OH$ complex, formed in step 3 and illustrated in the lower-left corner.

In the case of Au_3/MgO the situation is different. First of all the adsorption energy of the $O_2H\cdots OH$ complex is more than 50 % smaller on Au_3/MgO than on Au_1/MgO, see Fig. 5.8. At the same time the activation barrier for the formation of CO_2 is higher, making this step even slightly endothermic. This reaction becomes even more problematic, if one considers the bond dissociation energies of B2 - B4, cf. insets in Fig. 5.8, which are very close to the activation barrier. Hence it is quite likely that one of the bonds B2 - B4 breaks upon the impact of a CO molecule with a kinetic energy, necessary to overcome the reaction barrier. Still, if we assume for a moment that the bonds B2 - B4 will hold and the first CO_2 molecule is formed, than the remaining steps in the proposed catalytic cycle are exothermic and barrier free as shown in Fig. 5.8.

This concludes my investigations of Au_{1-4} on a regular MgO terrace. In the following two sections we concentrate on clusters in the gas phase.

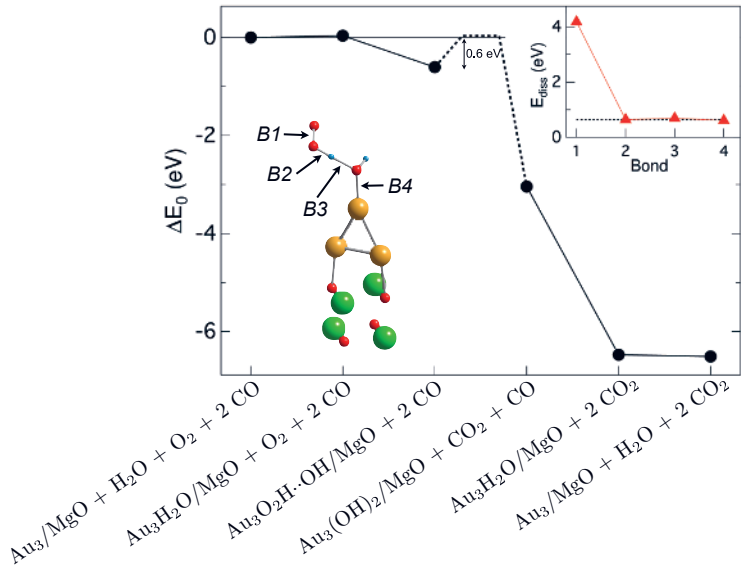

Figure 5.8: Change in the total energy during the successive adsorption of H_2O, O_2, and CO on Au_3/MgO to model the full catalytic cycle. The inset in the upper-right corner shows the bond dissociation energies of B1 - B4 (solid triangles) compared to the activation barrier (dotted line) of the $O_2H\cdots OH$ complex, formed in step 3 and illustrated in the lower-left corner.

5.2.2 The stability of Au_{13} and its potential for O_2 dissociation

Gold clusters containing 13 atoms are among the most studied systems for a number of different reasons. First, clusters containing 13, 55, and 147 atoms have closed shell structures and can therefore occur in high-symmetry geometries, such as icosahedral and cuboctahedral. The high-symmetry geometries of Au_{13} have been studied by theory for more than two decades [170–174]. It has been shown by theory as well that there exists quite a number of 'amorphous' structures of Au_{13}, which have a lower total energy than the high-symmetry isomers [153, 157, 175]. These findings of a rich potential energy surface is anticipated, since Au_{13} lies within the cluster size range, where the transition from planar to more compact three-dimensional structures occurs [176]. Anyhow, it has been recently found that the lowest energy structures have a common building block, i.e. a triangular prism as the center of Au_{13}, which is surrounded by a ring of the remaining seven atoms [177]. Different low-energy isomers differ only in the configuration of the atoms in the ring. The energy differences between these isomers are rather small, allowing for transitions between them [178]. These findings make the concept of an 'amorphous' ground state structure of Au_{13} obsolete.

Another aspect in the discussion of small gold cluster geometries is the importance of spin-orbit coupling for the relative stability of their isomers.

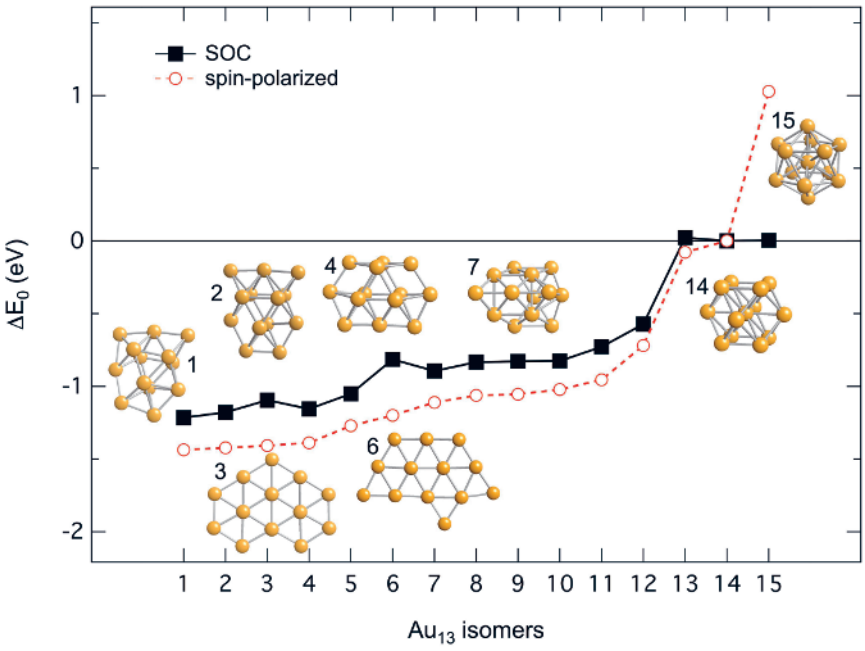

Figure 5.9: Relative stability of 15 Au_{13} isomers in the gas phase. Shown are the differences in the total energies ΔE_0 with respect to the cuboctahedral structure (no. 14). The energies from spin polarized calculations (open circles) and calculations including spin-orbit coupling (solid squares) are shown.

In Ref. [179] the transition from two- to three-dimensional structures has been predicted for clusters bigger than Au_{15}. But Au_{13} has not been included in that study. While Ref. [177] explicitly neglected spin-orbit coupling, it has been shown very recently that the inclusion of SOC favors the three-dimensional structures of Au_{13} over the two-dimensional ones [118]. Despite this methodological difference, Refs [177] and [118] have identified the same ground state geometry.

Although, these gold clusters are of interest in their own right, certainly of greater practical importance is their catalytic potential. In earlier studies, the adsorption of small molecules, such as O_2, CO, and H_2, on high-symmetry structures of Au_{13} has been studied [180, 181]. For the adsorption of various molecular species, foremost CO and O_2, different groups observed somewhat contradicting results [182–185]. In Ref. [183], for instance, a Au_{13} structure has been used, which appears to be rather close in energy to the triangular prism structures discussed above. Probably for this reason, it has been concluded in Ref. [183] that the studied Au_{13} structure is rather stable upon adsorption of e.g. an O_2 molecule. In another set of investigations on the Au_{13} mediated CO oxidation cycle, a Au_{13} structure has been used, which is energetically further away from the ground state [182, 184, 185]. Due to

the chosen structure, Refs [182, 184, 185] have found significant structural changes upon molecular adsorption.

In paper III, we systematically address the discrepancies between Ref. [183] and Refs [182, 184, 185] by showing that the ground state structure of Au_{13} is rather stable upon adsorption of an O_2 molecule.

In a first step, we perform density functional theory calculations of 15 distinct Au_{13} isomers in order to investigate their relative stabilities and potential chemical reactivities.

In accordance with Refs [118, 177], we find three-dimensional structures, that contain a triangular prism in their center which is surrounded by a ring of the remaining seven atoms, to be the most stable isomers of the 13-atom gold cluster. In Fig. 5.9 the total energies of the 15 isomers with respect to the total energy of the cuboctahedral isomer are shown, both for a spin polarized calculation and for one that also takes SOC into account. Spin-orbit coupling clearly favors some of the studied three-dimensional structures over the considered two-dimensional ones. In addition, we find the icosahedral structure to be unstable once SOC is included and it relaxes into the cuboctahedral structure instead.

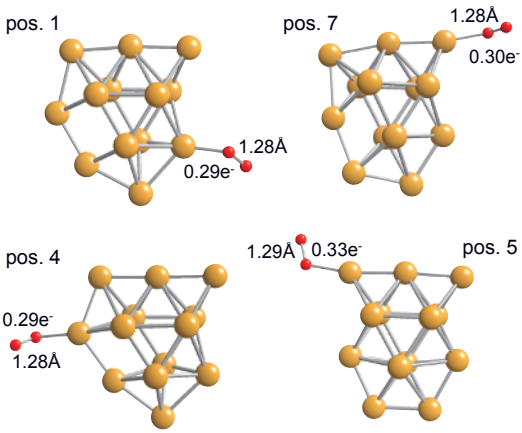

Figure 5.10: Illustration of the relaxed $Au_{13}O_2$ structures with the highest binding energies of O_2. Also shown are the additional Bader charges, donated into O_2 and the O-O bond lengths (the equilibrium O-O distance is 1.23 Å).

Starting from the ground state structure no.1, we study the binding of O_2 to Au_{13} and find the geometry of the ground state structure to be generally stable. Only for one binding site, we find that Au_{13} transforms into a very similar isomer upon adsorption of O_2, see Fig. 5.10. In order to shed some light on the catalytic potential of Au_{13}, we also study the separate adsorption of two oxygen atoms in the vicinity of one of the favored O_2 binding sites. For this particular site, we find that the dissociation of the adsorbed oxygen molecule is exothermic, since the total energy of the system is decreased

by 0.47 eV. Further investigations into the oxygen dissociation and the catalytic activity of this cluster are desirable.

5.2.3 Thermally excited vibrations in Cu, Ag, and Au trimers

In paper IV we present a density functional theory study of potential energy surfaces of charged and neutral copper, silver, and gold trimers with special emphasis on the geometries accessible at elevated temperatures (T > 0 K), since thermally excited vibration modes can play an important role for the physical and chemical properties of these small clusters. The coupling strength of a thermal bath to a quantum mechanical system is in the order of $k_B T$. Therefore, thermally accessible states at room temperature (T = 298 K) are located within a 25 meV range from the ground state. In real applications, for instance in catalytic converters used in vehicles, temperatures as high as 1000 K are possible, which would give a 80 meV range of thermally accessible geometries.

The parameter scans of the energy surfaces and the ground state structures are determined with the projector augmented-wave method including spin-orbit coupling. The obtained potential energy maps for charged clusters are quite similar for the studied elements, whereas the neutral clusters have rather different potential energy surfaces.

The potential energy surfaces of the cationic trimers have one minimum, which is localized around the 60° ground state geometry with D_{3h} symmetry. We find that a thermal energy of 25 meV allows for up to 5 percent deviations from the equilibrium bond length at 0 K.

In case of the anionic trimers, the extra electron causes repulsion, resulting in one minimum in their potential energy surface around the linear $D_{\infty h}$ symmetry. The range of thermally accessible bond lengths for the anionic trimers at room temperature is also about 5% for bond stretching, respective compression, with respect to the ground state configuration.

For neutral Cu_3 the energy surface exhibits one fairly deep energy minimum, see Fig. 5.11 (upper panel). In the case of Ag_3, Fig. 5.11 (middle panel), the surface is comparatively flat. It has two shallow minima separated by an energy barrier of 20 meV only. Hence, for Ag_3 there exist many thermally accessible geometries in a wide range of angles and bond lengths already at room temperature.

For Au_3, two distinct energy minima appear, see lower panel in Fig. 5.11, one with the apex angle of 60° and the other with 148°. The 148° trimer is the lowest energy configuration of Au_3, being 28 meV lower in energy than the 60° structure. Both minima are well-separated by a barrier of 180 meV.

The trimers have $3N - 6 = 3$ normal vibrational modes, two of which are illustrated in Fig. 5.12. Choosing Au_3 as a case study, we explore its thermally accessible geometries along the active normal modes of Au_3 and their reactivity with a CO molecule, see Fig. 5.12 for illustrations. Depending

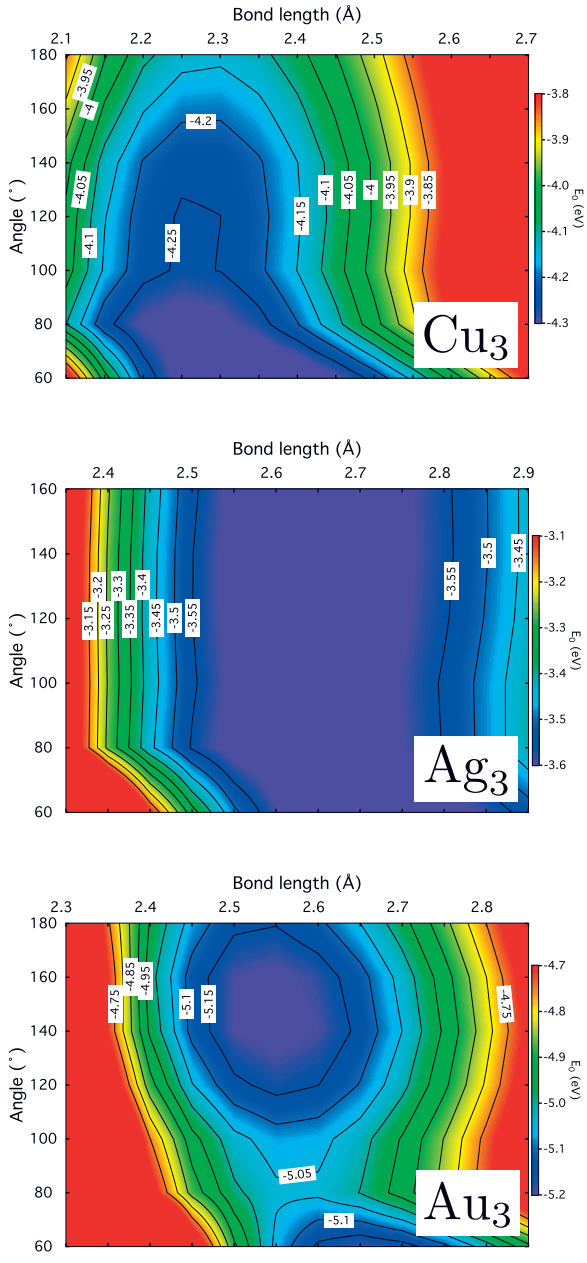

Figure 5.11: Scans of the Born-Oppenheimer potential energy surfaces of the neutral copper (upper panel), silver (middle panel), and gold trimer (lower panel) with respect to the apex angle α and the symmetric bond lengths $a = c$, see Fig. 5.12. Note that the range of the color-coded energy scales is 0.5 eV.

on the Au_3 isomer and the considered binding site for the CO, we find binding energies of the molecule between -0.95 and -1.88 eV. The charge transfer from the gold trimer into CO is approximately 0.1 e^-, which is comparable to the values found in paper I.

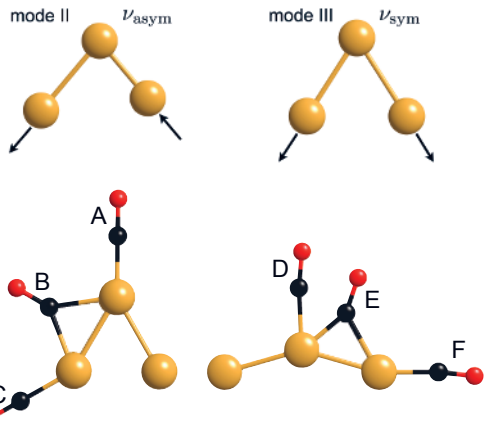

Figure 5.12: Upper row: Illustration of the asymmetric (II) and symmetric (III) vibration mode. Lower row: the six considered binding sites of CO on the 60° and 148° isomer of Au_3.

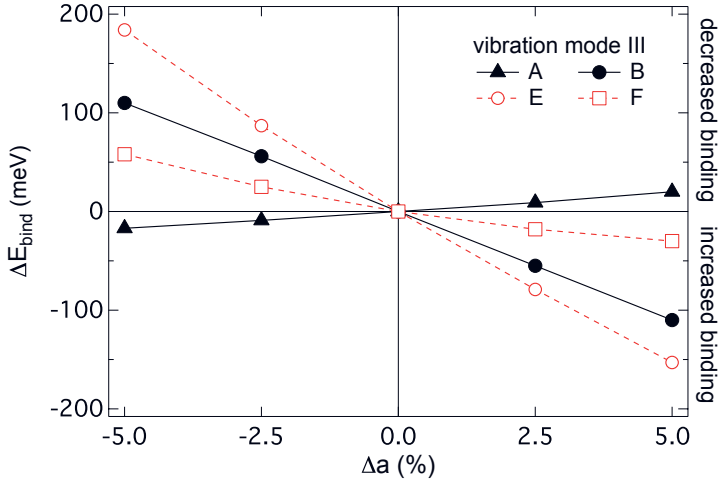

Figure 5.13: Change in the binding energies of CO on Au_3 along geometries in the symmetric vibration mode III, see Fig. 5.11. Δa is the relative bond length contraction/stretching versus the bong length in the ground state. ΔE_{bind} is the change in the binding energy of CO compared to E_{bind} in the ground state structure.

In order to calculate the CO binding energies in the case of thermally excited modes, we performed calculations for a number of trimer geometries

along the normal modes of asymmetric (II) and symmetric (III) vibrations for the two structures (60° and 148°), which correspond to the two energy minima, see lower panel in Fig. 5.11. The bond lengths a were chosen to be ± 2.5 and ± 5 % of the equilibrium distances, which are 2.655 Å for the 60° structure and 2.545 Å for the 148° structure. To obtain the cluster geometries for asymmetric mode II, one bond length was fixed to $a \pm 2.5(\pm 5)$ %, while the other was allowed to relax along the vibration direction.

The changes in the binding energy of CO for the symmetric vibrational mode III are shown in Fig. 5.13. There, one finds a significant enhancement of up to 150 meV of the CO binding energy to the excited Au_3 geometries, which are accessible already at room temperature, see Fig. 5.13 position F.

To conclude, our results in paper IV suggest that initial binding of a molecule can be energetically more favorable, and thus more probable to occur, for distorted cluster configurations away from the ground state structure, which are realized due to the activation of the vibration modes at elevated temperatures.

This concludes the summary of papers I - IV on nanocatalysis by gold. In the following section, which summarizes papers V and VI, the focus is still an small gold clusters and coinage metal atoms, but now on graphene as a substrate instead.

5.3 Coinage metals on graphene

Graphene, a single layer of carbon, stands out as an extraordinary material that offers enormous possibilities for applications in electronics, sensors, biodevices, catalysis, and energy storage [122–124, 186]. The gapless ultrarelativistic energy spectrum of graphene [186] as well as effects such as Klein tunneling [187] are of fundamental interest from a theoretical point of view. Moreover, graphene shows the Quantum Hall effect at room temperature [188] and its conductive properties correspond to ballistic transport.

Historically, carbon allotropes, e.g. graphite, carbon nanotubes, and fullerene have been extensively used for studying the absorption processes of finite-sized particles on them. Small coinage metal clusters on graphene have been first used to model the adsorption on graphite surfaces or single-walled carbon nanotubes [189–191]. After the experimental evidence for the existence of graphene has been found by Novoselov et al. [120, 121] the study of cluster adsorption on graphene became important in its own right.

For the utilization of these systems a deeper understanding of their stability and electronic properties is needed. In the following two sections, our investigations of some fundamental aspects of Au_{1-4} (paper V) as well as coinage metal adatoms (paper VI) on graphene are summarized,

5.3.1 Mobility and clustering of Au_{1-4}

Motivated by the experimentally observed high mobility of gold atoms on graphene and their tendency to form nanometer-sized clusters [125], we present in paper V a density functional theory study of the ground state structures of small gold clusters on graphene, their mobility and clustering. The calculated ground state structures of Au_{1-4} on graphene are shown in Fig. 5.14, along with the Bader charges of in the individual gold atoms and the most relevant bond lengths.

While the clusters containing up to three gold atoms have one unambiguous ground state structure, both gas phase isomers of Au_4 can be found on graphene, cf. Fig. 5.14. In the gas phase the diamond shaped Au_4^D cluster is the ground state structure, whereas the Y shaped Au_4^Y becomes the actual ground state when adsorbed on graphene.

Figure 5.15 (a) shows the adsorption energies of the considered clusters on graphene, which range from -0.1 to -0.59 eV. The lower panel (b) of the same figure shows also the charge transfer from the carbon atoms around the adsorption site into the gold clusters. Compared to 0.3 e^- per Au-O, which we find in paper I, these charge donations are significantly smaller in the case of graphene, i.e. up to 0.12 e^- in the case of Au_4^Y.

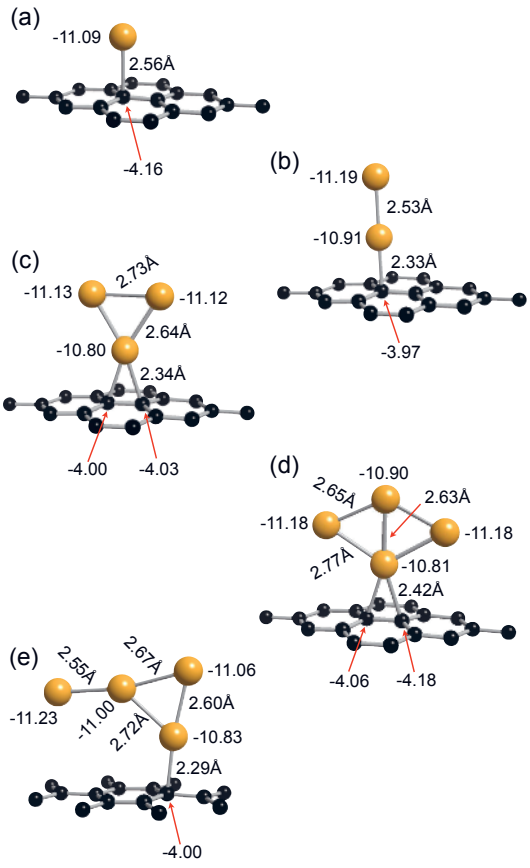

Figure 5.14: Ground state structures of Au_{1-4} on a 5×5 graphene sheet. Structures (a)-(d) were obtained by soft-landing the clusters from the gas phase. The isomer Au_4^Y (e) is formed by clustering two pre-adsorbed dimers. It is 137 meV lower in energy than Au_4^D/graphene (d). Also given are relevant bond lengths and Bader charges. Note: in our calculations neutral Au atoms have a Bader charge of -11 and C atoms of -4, respectively. The different atom species are illustrated as yellow (Au) and black (C), respectively.

We show that both isomers of Au_4 can be produced by two distinct clustering processes on graphene, i.e. by adding a single gold atom at a time (Au_4^D) and by fusing two dimers (Au_4^Y), respectively.

Figure 5.16 shows the differences in the total energies of the clusters at different sites, i.e. top, bridge, and in between those two. The diffusion barriers of all studied clusters range from 4 to 36 meV only. This explains the high mobility of Au_{1-4} along the C-C bonds of graphene even at very low temperatures.

We also study the stepwise formation of a gold dimer out of two pre-adsorbed adatoms in detail. We find the graphene mediated, attractive

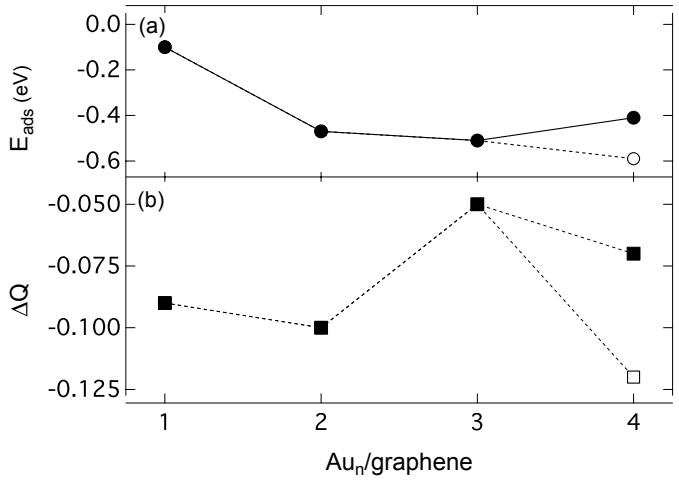

Figure 5.15: Upper panel (a): Cluster adsorption energy of Au_{1-4} on graphene. Lower panel (b): total charge transferred from the graphene sheet into the clusters, calculated by the Bader analysis. Full symbols: gas phase structures adsorbed on graphene, cf. Figs 5.14 (a) - (d). Open symbols: Y shaped Au_4^Y/graphene, cf. Fig. 5.14 (e).

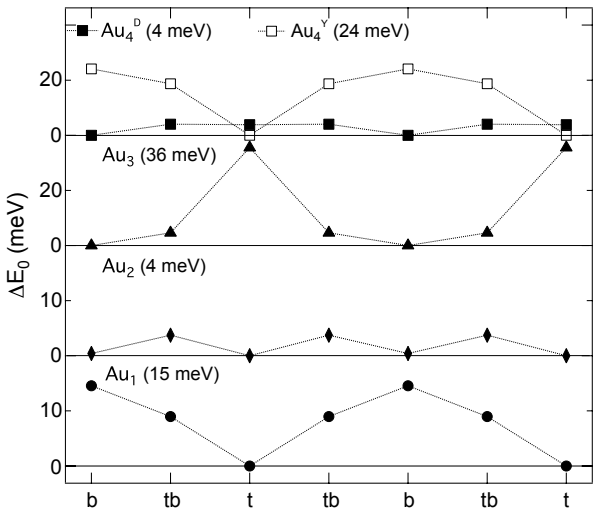

Figure 5.16: Difference in the total energies ΔE_0 at the top (t), bridge (b), and a positions in between (tb) of Au_{1-3} and $Au_4^{Y,D}$ on graphene. E_0 of the respective cluster ground state was subtracted to show the diffusion barriers along the C-C bonds (also given in parenthesis). Note the smaller scales for $Au_{3,4}$.

interaction of two gold adatoms to have a range of approximately 4.3 Å, which is clearly longer than in the gas phase, see Fig. 5.17.

In summary, our analysis of the electronic structures of Au_{1-4}/graphene in paper V identifies the opportunity to form strong gold-gold bonds and the

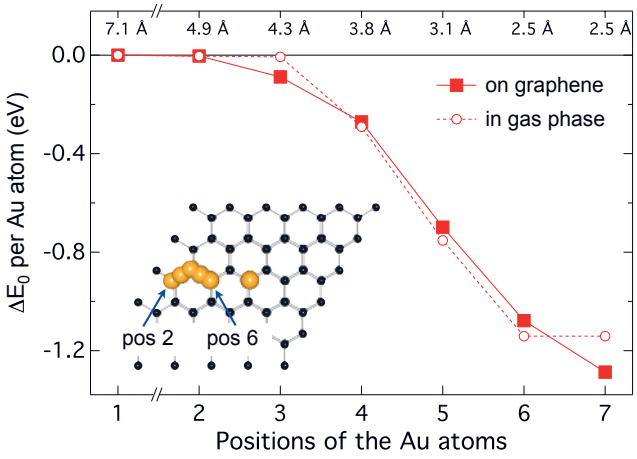

Figure 5.17: Changes in the total energy ΔE_0 when forming Au_2/graphene from two pre-adsorbed adatoms (solid symbols) and for the dimer formation in the gas phase (open symbols). The x-y coordinates of the Au adatoms were kept fixed for positions 1-6. The system relaxes without an additional activation barrier from position 6 to 7, the dimer ground state structure, cf. Fig. 5.15 (b). The Au-Au distances for the different positions are given on the top axis.

graphene mediated interaction of the pre-adsorbed fragments as the driving forces behind gold's tendency to aggregate on graphene.

5.3.2 The van der Waals interactions between graphene and Cu, Ag, and Au adatoms

As of today, it is still a challenge for theory to correctly predict the binding of atoms and molecules on coinage metal surfaces [192]. Recently reported studies, employing a variety of methods, showed the importance of non-local correlations for the correct description of the physisorption of aromatic molecules on copper, silver, and gold surfaces [100–103]. Also the reverse setup of coinage metal atoms and clusters on carbon-based materials such as graphite is a long-standing and not completely resolved issue. Already Darby et al. [193] speculated that dispersion forces, i.e. van der Waals forces, significantly contribute to the adsorption energies of gold atoms on graphite.

To address the question, we present in paper VI our systematic density functional study of the adsorption of copper, silver, and gold adatoms on graphene, especially accounting for van der Waals interactions by the vdW-DF and the PBE+D2 methods. In particular, we analyze the preferred adsorption site (among top, bridge, and hollow positions) together with the corresponding distortion of the graphene sheet and identify diffusion paths.

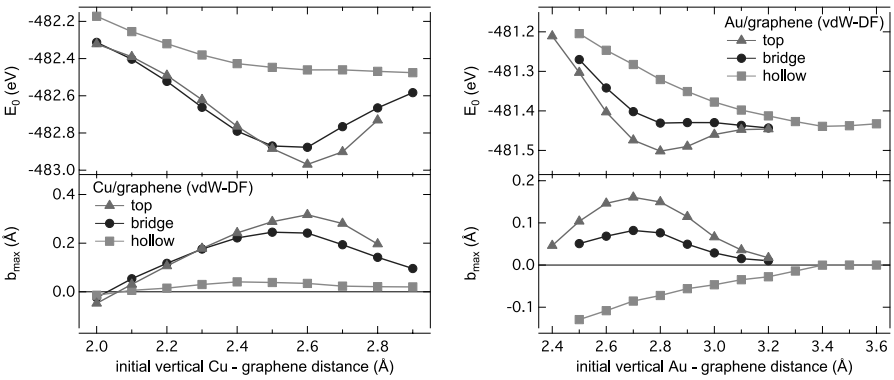

Figure 5.18: Upper panels: total energies of copper (left) and gold (right) vs. initial vertical adatom - graphene distance for three binding sites, calculated in vdW-DF. Lower panels: vertical distortion ($b_{\max}$) of the carbon atoms closest to the adatom adsorption site.

Both vdW schemes show that the coinage metal atoms do bind to the graphene sheet and that in some cases the buckling of the graphene can be significant. For copper and gold we find that the PBE parametrization to the exchange-correlation energy predicts the same ordering of the adsorption sites as vdW-DF and PBE+D2, i.e. it also favors the top over the bridge and hollow positions, see Fig. 5.18. We also find that the non-local interactions increase the calculated adsorption energies of Cu and Au on graphene by up to 0.8 eV (PBE+D2) and 0.45 eV (vdW-DF), respectively, see Fig. 5.18. The predicted vertical equilibrium distance calculated with PBE, for Cu and Au adsorption, agrees to better than 13% with the more advanced non-local methods. The buckling, i.e. vertical distortion, of the graphene sheet at the adsorption site is of the order of 50% smaller when the structural relaxation is performed in the PBE+D2 method compared to relaxations with PBE only.

For the adsorption of silver on graphene our calculations suggest that it is purely of van der Waals type, see Fig. 5.19. Different generalized gradient approximations to the exchange-correlation functional fail to give any binding at all, while the PBE+D2 and vdW-DF predict physisorption at large equilibrium distances of 2.9 and 3.3 Å, respectively, see Fig. 5.19.

However, we observe also some quantitative differences between the vdW-DF and the PBE+D2 methods. For instance the adsorption energies calculated with the PBE+D2 method are systematically higher than the ones obtained with vdW-DF. Moreover, the equilibrium distances computed with PBE+D2 are shorter than those calculated with the vdW-DF method.

From the differences in the total energies we conclude that diffusion of Cu and Au takes place along the carbon-carbon bonds, while the Ag adatoms can diffuse almost unrestricted on the graphene sheet. Especially, the result for

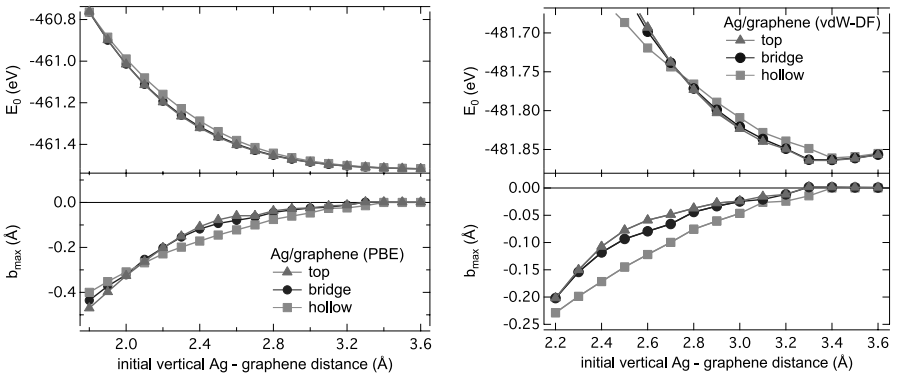

Figure 5.19: Upper panels: total energies vs. initial vertical Ag - graphene distance for three binding sites, calculated in vdW-DF (left) and PBE (right). Lower panels: vertical distortion ($b_{\max}$) of the carbon atoms closest to the Ag adsorption site.

Au justifies the usage of PBE in paper V, where the mobility and clustering of small gold clusters on graphene is studied.

The final chapter (Chap. 6) concludes this Thesis and gives an outlook to potentially interesting continuations of my work, that was presented here.

6. Conclusions and outlook

In addition to experiment and pure theory, computational physics evolved into the third main branch of physics during the last decades. In condensed matter, surface and cluster physics, density functional theory proved to be a reliable tool for understanding and describing matter on its atomic to nanometer scale. Moreover, the accurate prediction of materials properties and chemical processes became possible, thanks to the combination of feature-rich implementations of density functional theory and powerful computers. Understanding nanocatalysis, in particular, is hardly imaginable without these developments.

I would like to conclude by pointing out some problems that seem to be interesting continuations of the work presented in this Thesis.

If one is interested in graphene as a substrate for cluster deposition, the properties of a perfect graphene sheet need to be thoroughly understood. However, such a model system is only a first approximation to real samples. Further questions, such as vacancies in graphene or its chemical functionalization, gained already a lot of attention. Also graphene itself is often supported by semiconductors or metals. In this way one tries to induce desired changes in its electronic structure, e.g. the opening of a small gap at the Fermi level.

In recent experiments, it has been observed that the final size of gold aggregates, grown on a stack of a few graphene sheets, depends on the number of sheets. These layered systems are in between pure graphene and graphite and the inclusion of van der Waals forces certainly needs to be taken into account for this sparse system.

As we observed for the coinage metal trimers in the gas phase, thermally excited vibrations can play an important role for the reactivity of the clusters. However, these vibrations have been widely neglected in density functional theory calculations so far. Continuing along these lines of thought, it would be of considerable interest to address questions like: what happens to the reaction energy when carbon monoxide is oxidized on a small supported gold cluster? Molecular-dynamics simulations, although computationally expensive, already allow to study these dissipation phenomena for small systems on a time-scale of a few dozen picoseconds.

Defective oxide surfaces are certainly a worthwhile subject in its own right. Surface vacancies have been identified as a source of extra charge which can increase the catalytic activity of adsorbed metal clusters. On the other hand,

the importance of larger structural defects of the surface, such as edges, on the activity of clusters are less well studied yet.

The charge state of a cluster can also be controlled by depositing it on a layered metal / metal oxide structure. In particular, one can tune the charging of the cluster by varying the thickness of the metal oxide layer. Calculations can be more directly compared to such experiments, since it is possible to grow high-quality samples of layered substrates, which are regularly used for scanning tunneling microscopy. To proceed along these lines, one might even combine a metal and a defective metal oxide film to form a substrate for cluster deposition.

I modeled the heterogeneous catalysis of gas phase molecules on supported gold clusters with up to three molecules only, assuming an otherwise clean surface and no further molecules in the gas phase. Of course, in reality surfaces are very likely to be covered by adsorbed molecules even under the best high-vacuum conditions. Although much of the work in surface science is dedicated to these problems, many open question remain. The formation of the first layer of water on the stoichiometric rutile $TiO_2(110)$ surface is an archetypical example of a seemingly simple system. Very recently this systems was investigated again by means of photoelectron spectroscopy. The real-time measurements of oxygen 1s photoelectron spectra provided a detailed picture of how the hydroxyl to water ratio depends on the coverage. It was found that dissociation of the water molecules is the dominating process at low coverages, while molecular adsorption dominates at higher coverages. The O 1s spectra showed OH and H_2O growth rates indicative of nucleation of a specific OH-H_2O configuration over a substantial coverage range (0.05 - 0.40 ML). Quantitatively and qualitatively explaining the microscopical mechanism of this growth process is one of my current research projects.

Summarizing this Thesis, it can be stated that Bechstedt's theorem proved to be correct once more: the sum of all current physical problems is at least constant.

Acknowledgements

I would like to begin by giving my special thanks to my first supervisor Dr. Natalia V. Skorodomova. With her expertise, I could take my first steps into the land of surface science and cluster physics in the last two years of my Ph. D. studies. I will always be indebted for the opportunity to a fresh start and I hope that you also enjoyed our collaboration as much as I did!

I thank my second supervisor, Prof. Olle Eriksson for his inspirational ideas and discussions. May the van der Waals force always be with you!

Science is not a one man show and I have had great pleasure in sharing my excitement for physics with a number of collaborators and colleagues: Dr. Biplab Sanyal, Dr. Sébastien Lebègue, Dr. Anders Sandell, and Dr. Tomas Edvinsson. Also, Prof. Björgvin Hjörvarsson and Gunnar Pálsson, they make a living out of metal hydrides, for me it is a hobby (I take my hobbies seriously).

For the proof-reading of this Thesis, I am very thankful to Ute Cappel (commas, syntax, and plenty of helpful critical comments), Johan Falk (sammanfattning), and Pooja Panchmatia (this page).

The last five years I shared approximately 19.57% of my life with my office mates Mikael, Torbjörn, Peter, and Marcio. What else could one possibly ask for? We had it all. The whole spectrum from comradeship to days of silence for which I can only be thankful.

There is a good working atmosphere and environment in our department, which I would call 'Stimmung'. One always finds company for a coffee break, lunch or even just an informal discussion - thanks to all colleagues and guests, current and former, for their contribution.

I hope that even as a busy PhD student I managed to have a life and maintain my old and new friendships. Jörg, my oldest friend in town, how many shoes have we worn out on our walks to and from work? Ute and Stefan, I already miss our chats over a hot or cold beverage. Well, on second thought, the latter have been on average even more fun. All my other friends and acquaintances I thank for a whole lot of laughter and heated (political) debates. These have been the best mid-to-end twenties I ever have had!

Finally, my love Camilla, to whom I owe the most. Your love, support, and encouragement always gives me the strength to strive for the best! Thank you for just being you.

Last but not least, I am thankful to our child for staying put long enough for me to write these lines...

Sammanfattning

Den här avhandlingen presenterar resultaten av min forskning vid avdelningen för materialteori, ledd av professor Olle Eriksson, där jag under de senaste två åren undersökt en rad fysikaliska frågeställningar i området yt- och klusterfysik med doktor Natalia V. Skorodumova som huvudhandledare.

Både områdena yt- och klusterfysik är tämligen gamla, nästan 100 år i det första fallet. Förmågan att verkligen manipulera material på dess atomära nivå är däremot ganska nytt. Detta område kallas för nanovetenskap. Först med så kallade Scanning Tunneling-mikroskop blev det möjligt att till exempel förflytta enskilda atomer på en yta. Det mest kända exemplet för detta är kanske de tre bokstäverna I, B och M, som skrevs av 35 xenonatomer på en yta av nickel. Den här mikroskopiska världen styrs fullständigt av kvantmekanikens lagar som oftast ger oväntade egenskaper - lekmannen skulle nästan säga att dessa egenskaper är bakvända.

Mitt eget intresse har under de senaste två åren främst varit riktade mot en viss typ av små system, som är mindre än en nanometer, så kallde nanokatalysatorer. Till skillnad från vanliga katalysatorer följer deras egenskaper inga enkla lagar, såsom "om man höjer förhållandet från materialets yta till dess volym, så får du en bättre katalysator." Istället kan en enda atom i en nanokatalysator förändra dess egenskaper och förmågor dramatiskt.

För att studera dessa system har jag först och främst använt beräkningsmetoder som bygger på den så kallade täthetsfunktionalteorin. En implementering av den teorien i ett datorprogram, så som VASP, gör det möjligt att beräkna den elektroniska strukturen av ett godtyckligt material. Den elektroniska strukturen bestämmer en hel rad andra fysikaliska och kemiska egenskaper, till exempel om ett material är en metall eller om ett kluster kan fungera som katalysator för en viss kemisk reaktion. Det betyder att dessa metoder kan användas för att (1) tolka och bättre förstå mikroskopiska mekanismer i befintliga experimentella resultat, samt (2) förutspå och skräddarsy nya material i datorn. Mina projekt tillhör i första hand den första kategorien.

Avhandlingen består huvudsakligen av två delar: en mer allmänt skriven introduktion av metoderna som använts och deras härkomst (kapitel 2 - 4) och en sammanfattning av mina projekt (dvs artikel I - VI) i kapitel 5. Fullständiga manuskript är bifogade i den tryckta versionen av avhandlingen.

Artikel I och II behandlar de minsta möjliga guldklustren, bestående av bara en till fyra atomer, på ett underlag av magnesiumoxid. Förutom deras elektroniska och geometriska strukturer undersöktes hur de adsorberar kolmonoxid och syremolekyler. Detta ledde till vår förklaring till varför de minsta två klustrena, $Au_{1,2}$, inte kan oxidera CO. De två större klustrena, $Au_{3,4}$, är å andra sidan tillräckligt stora för att samtidigt adsorbera båda molekylsorter som kan leda till en oxidationsreaktion, så som observationer i experiment tidigare visat. I artikel II undersöks om en vattenmolekyl kan ha positiv inverkan på CO-oxidationen ovan. Även om det kan formas ett mycket aktiverat O_2H-OH-komplex på $Au_{1,3}$ är det mycket sannolikt att det dissocieras under inverkan av CO då dess bindningar är för svaga samt att restkomplexet $(OH)_2$ inte är stabilt.

Metallkluster bestående av 13 atomer undersöktes redan på 1980-talet. Guldklustret Au_{13} visar sig har många två- och tredimensionella strukturer med liknande energi i sin gasfas. Vi har undersökt hur spin-bankopplingen och adsorptionen av en syremolekyl påverkar stabiliteten och strukturen av Au_{13}. Det visade sig att klustret enkelt kan binda och aktivera en syremolekyl. Även en dissociation i två enskilda syre atomer är energetiskt möjligt, vilket är mycket intresssant för en hel del kemiska reaktioner - så som den ovan nämnde CO oxidationen.

I artikel IV behandlar vi en aspekt som hittills försummats i teoretiska undersökningar för små ädelmetallkluster: hur deras termiska vibrationer kan förbättra bindningen av till exempel CO. Detta understryker hur kemiska reaktioner kan bli lättare när man höjer temperaturen för reaktionen.

Artikel V behandlar också små guldkluster och artikel VI ädelmetallatomer (Cu, Ag, Au) på grafén - ett ämne som blivit mycket populärt under de senaste åren. Tidigare experiment har visat att guldatomer på grafit och grafén är mycket rörliga och lätt formar större strukturer. Jag har undersökt rörlighet för Au_{1-4} på grafén och hur de större klustrena kan bildas av mindre (Artikel V). Sedan 1970-talet har experimentalister misstänkt att van der Waal-kraften är huvudansvarig för bindningen mellan grafit och ädelmetallatomer och -kluster, så som Cu, Ag och Au. Det skulle i så fall också vara relevant för deras adsorption på grafén. Under senaste åren har det blivit möjligt att ta hänsyn till van der Waal-kraften inom implementeringar av täthetsfunktionalteorin. Vi har använt två olika metoder för att studera Cu, Ag, och Au:s adsorption på grafén och kunde visa att det är endast för silver som van der Waal-kraften är fullständigt ansvarig för bindningen till ytan (Artikel VI).

Zusammenfassung

Die vorliegende Arbeit ist Ergebnis meiner insgesamt fünfjährigen Forschungstätigkeit an der Universität zu Uppsala in der Gruppe für Materialtheorie von Prof. Dr. Olle Eriksson.

Bereits während meiner Jugend hegte ich den Wunsch Physik zu studieren. Zwar bedurfte es zu dieser Zeit einer leidlichen Überzeugung, doch einmal für diese für sie etwas befremdliche Idee gewonnen, unterstützen mich meine Eltern nach Kräften bei der Verwirklichung meiner Ziele. Hierfür gebührt ihnen auf immer mein tiefer Dank.

Meine ersten Gehversuche auf dem Gebiete der Computerphysik unternahm ich für meinen Beitrag im Wettbewerb "Jugend forscht" im Jahre 1997. Mein damaliger Physiklehrer am Gymnasium Carolinum zu Bernburg, Maik Burgemeister, ermöglichte mir zu diesem Zwecke die parallele Ausführung meiner Simulation auf allen neu beschafften 100 MHz Pentium PCs des Computerkabinetts, was meine Datengrundlage erheblich verbreiterte.

Nach sechs Semestern des Studiums der Physik, sowie einigen Ausflügen in die Philosophie und Mathematik, an der Friedrich Schiller Universität zu Jena, begab ich mich zum Wintersemester 2003 als Austauschstudent nach Uppsala. Meine Diplomarbeit mit dem Titel "Supraleitende Quantenbits als ein Beispiel für dissipative Quantensysteme" fertigte ich 2005 unter der Anleitung von PD Dr. Wolfram Krech am Institut für Festkörperphysik an der FSU zu Jena an.

Einmal in der Festkörperphysik angelangt, lag es nahe, in diesem facettenreichen Teilgebiete der Physik auch ein Promotionsstudium anzustreben. Zunächst studierte ich unter Prof. Dr. Peter M. Oppeneer die elektronischen und magnetooptischen Eigenschaften verschiedener Metalllegierungen, wie der sogenannten Heuslerschen und solcher, welche Uran zu ihren Bestandteilen zählen.

Nach dem Erhalt meines Licentiats begann ich im Herbst des Jahres 2008 meine gegenwärtigen Forschungen im Bereiche der Oberflächen- und Clusterphysik unter der Betreuung von Dr. Natalia V. Skorodumova. Beides sind bereits vergleichsweise alte Forschungsgebiete. Während der vergangen Jahrzehnte erlaubte jedoch die Entwicklung neuartiger experimenteller Methoden, wie des Rastertunnelmikroskops, nicht nur das Betrachten von Oberflächen mit einer atomarer Auflösung, sondern vielmehr auch die gezielte Manipulation einzelner Atome. Das Bild von 35 Xenonatomen,

die auf einer Nickeloberfläche zu den drei Buchstaben I, B und M geformt worden, legt davon beredtes Zeugnis ab.

Aus der mannigfaltigen Zahl nanometergroßer Systeme beschäftigten mich in den vergangenen beiden Jahren vornehmlich die so genannten Nanokatalysatoren. Im Gegensatze zu gewöhnlichen Katalysatoren, wie man sie in etwa in benzingetriebenen Kraftfahrzeugen vorfinden kann, gehorchen Nanokatalysatoren in aller Regel keinen einfachen Gesetzmäßigkeiten, wie etwa einem direkten Zusammenhang ihres katalytischen Leistungsvermögens mit ihrem Verhältnis von Oberfläche zu Volumen. Vielmehr kann das bloße Hinzufügen oder Entfernen eines einzigen Atomes, die Eigenschaften eines Nanokatalysators auf das dramatischste verändern.

Zum allgemeinen Verständnisse der Materie in ihrer festen kristallinen Phase, sowie der eben benannten davon ableitbaren Systeme, bedarf es zunächst nur der Gesetze der Quantenmechanik und der elektrostatischen, d.i. Coulombschen, Kraft. Im Grunde bestimmen diese Gesetzmäßigkeiten die Dynamik der Elektronen im betrachteten Materiale, woraus sich dann eine ganze Reihe weiterer physikalischer und vor allem auch chemischer Eigenschaften ableiten lassen. Auf diese Art und Weise lässt sich zum Beispiel die Frage beantworten, ob dieses Material ferromagnetisch sei oder jenes chemische Reaktionen katalytisch beschleunigen könne.

Die dynamischen Gesetze der Quantenmechanik, etwa in Form der Schrödingerschen Gleichung, beschreiben die Bewegung aller mikroskopischen Teilchen, also auch der Elektronen. Obgleich eine Lösung solcher Gleichungen stets existiert, wie uns die Mathematik lehrt, so ist es außer in den einfachsten Fällen praktisch unmöglich diese exakten Lösungen auch aufzufinden. In Fällen wie diesen bedient sich der Physiker gern eines Kniffs: er formuliert das praktisch unlösbare Problem kurzerhand in ein mehr zugängliches um, wobei sich freilich der physikalische Inhalt nicht ändern darf, um die Gültigkeit der Ergebnisse zu bewahren. Die sogenannte Dichtefunktionaltheorie, die von der Dichte der Elektronen anstatt deren Vielteilchenwellenfunktion ausgeht, leistet dies im Falle der Schrödingerschen Gleichung.

Während meiner Zeit als Doktorand bestand nun meine Forschung darin, mit Hilfe von weit entwickelten Computerprogrammen, welche die Dichtefunktionaltheorie umsetzen, auf Großrechenanlagen die elektronische Struktur der verschiedenen oben genannten Materialien zu berechnen, um daraus weitere physikalische und chemische Eigenschaften erklären und vorhersagen zu können. Bereits der Titel der vorliegenden Arbeit steckt dabei den Rahmen des Forschungsgegenstandes ab: "Die Anwendung der Dichtefunktionaltheorie zum Studium kleiner auf einem Substrate gelagerter Goldpartikel und verwandte Fragestellungen - welchen Unterschied ein einziges Atom ausmacht."

In den sechs Manuskripten, die der gedruckten Fassung dieser Arbeit beigefügt sind, beschäftige ich mich zuförderst mit grundlegenden

physikalischen und auch katalytischen Eigenschaften von kleinsten Goldpartikeln, sogenannten Mikroclustern. Perspektivisch soll hierbei die Frage Beantwortung finden, ob diese Partikel sich als die oben beschriebenen Nanokatalysatoren, etwa für die Oxidation von Kohlenstoffmonoxid, eignen. Die untersuchten Goldpartikel sind entweder auf einer Magnesiumoxidoberfläche (Manuskripte I und II) oder einer nur eine Atomlage dünnen Kohlenstoffschicht, d.i. Graphen, dem zweidimensionalen Baustein von Graphit, gelagert (Manuskripte V und VI). In den Manuskripten III und IV werden 13-atomige Goldpartikel bzw. Kupfer-, Silber- und Goldtrimere in der Gasphase untersucht. Jenseits der fachtypischen Fragestellungen nach dem energetischen Grundzustande und dergleichen, untersuchen wir in den ersten vier Manuskripten ebenfalls, inwiefern diese Goldpartikel einfache Moleküle, wie Sauerstoff, Kohlenstoffmonoxid oder auch Wasser an sich binden können und ob dies einer katalytischen Reaktion, etwa der Oxidation von Kohlenstoffmonoxid zu Kohlenstoffdioxid, förderlich sei. Die Goldpartikel auf der Magnesiumoxidoberfläche erwiesen sich hierbei in der studierten Konfiguration als zu diesem Zwecke ungeeignet. Andererseits zeigen die Partikel in der Gasphase ein gewisses reaktives Potenzial, etwa für die erwähnte Oxidation von Kohlenstoffmonoxid.

Im fünften Manuskripte stehen vornehmlich die hohe Beweglichkeit kleinster Goldpartikel und deren Aggregationsmechanismen auf dem Graphen im Vordergrunde. Schließlich beantworten wir im sechsten und letzten Manuskripte die sehr grundlegende Frage nach der Bedeutung der van der Waalschen Bindungskräfte für die Adsorption von Kupfer-, Silber- und Goldatomen auf dem Graphen. Dabei stellte sich unter anderem heraus, dass allein die van der Waalschen Kräfte für die Bindung des Silbers auf dieser Kohlenstoffoberfläche verantwortlich sind, es sich somit in diesem Falle um eine reine Physisorption handelt.

Uppsala, im Oktober 2010

Martin Amft

7. Bibliography

[1] F. Braun. Ueber ein Verfahren zur Demonstration und zum Studium des zeitlichen Verlaufes variabler Ströme. *Ann. Phys.*, 296:552, 1897.

[2] J. J. Thomson. Cathode Rays. *Philos. Mag.*, 44:293, 1897.

[3] J. J. Thomson. On the charge of electricity carried by the ions produced by Röntgen rays. *Philos. Mag.*, 46:528, 1898.

[4] J. J. Thomson. On the theory of the conduction of electricity through gases by charged ions. *Philos. Mag.*, 47:253, 1899.

[5] J. J. Thomson. On the structure of the atom: an investigation of the stability and periods of oscillation of a number of corpuscles arranged at equal intervals around the circumference of a circle; with application of the results to the theory of atomic structure. *Philos. Mag.*, 7:237, 1904.

[6] A. Einstein. Die von der Molekularkinetischen Theorie der Wärme Geforderte Bewegung von in ruhenden Flüssigkeiten Suspendierten Teilchen. *Ann. Phys.*, 17:549, 1905.

[7] J. Perrin. Le Mouvement Brownien et la Réalité Moleculaire. *Ann. Chimi. Phys.*, 18:5, 1908.

[8] H. Geiger and E. Marsden. On a Diffuse Reflection of the α-Particles. *Proc. R. Soc. London, Ser. A*, 82:495, 1909.

[9] E. Rutherford. The scattering of α and β particles by matter and the structure of the atom. *Philos. Mag.*, 21:669, 1911.

[10] N. Bohr. On the constitution of atoms and molecules. *Philos. Mag.*, 26:1, 1913.

[11] N. Bohr. On the constitution of atoms and molecules. *Philos. Mag.*, 26:476, 1913.

[12] N. Bohr. On the constitution of atoms and molecules. *Philos. Mag.*, 26:857, 1913.

[13] A. Sommerfeld. Zur Quantentheorie der Spektrallinien. *Ann. Phys.*, 356:1, 1916.

[14] A. Sommerfeld. Zur Quantentheorie der Spektrallinien. *Ann. Phys.*, 356:125, 1916.

[15] I. Langmuir. Chemical Reactions at Low Pressures. *J. Amer. Chem. Soc.*, 37:1139, 1915.

[16] I. Langmuir. Dissociation of hydrogen into atoms. *J. Amer. Chem. Soc.*, 34:860, 1912.

[17] I. Langmuir. Chemical Reactions at Very Low Pressures. I. The Clean-up of Oxygen in a Tungsten Lamp. *J. Amer. Chem. Soc.*, 35:105, 1913.

[18] I. Langmuir. Chemical Reactions at Very Low Pressures. II. The Chemical Clean-up of Nitrogen in a Tungsten Lamp. *J. Amer. Chem. Soc.*, 35:931, 1913.

[19] A. Bravais. *Études cristallographiques. I: Du Cristal considéré comme un simple assemblage de points*. Gauthier-Villars, Imprimeur-Libraire, Paris, 1866.

[20] A. Bravais. *Études cristallographiques. II: Du Cristal considéré comme un assemblage de molécules polyatomiques*. Gauthier-Villars, Imprimeur-Libraire, Paris, 1866.

[21] W. Friedrich, P. Knipping, and M. Laue. Interferenz-Erscheinungen bei Röntgenstrahlen. *Ann. Phys.*, 346:971, 1912.

[22] W. L. Bragg. The Specular Reflection of X-rays. *Nature*, 90:410, 1912.

[23] I. Langmuir. The Adsorption of Gases an Plane Surfaces of Glass, Mica and Platinum. *J. Amer. Chem. Soc.*, 40:1361, 1918.

[24] I. Langmuir. Chemical Reactions on Surfaces. *Trans. Faraday Soc.*, 17:607, 1921.

[25] M. Planck. Ueber das Gesetz der Energieverteilung im Normalspectrum. *Ann. Phys.*, 309:553, 1901.

[26] P. Lenard. Ueber die lichtelektrische Wirkung. *Ann. Phys.*, 313:149, 1902.

[27] A. Einstein. Über einen die Erzeugung und Verwandlung des Lichtes betreffenden heuristischen Gesichtspunkt. *Ann. Phys.*, 322:132, 1905.

[28] A. H. Compton. A Quantum Theory of the Scattering of X-Rays by Light Elements. *Phys. Rev.*, 21:483, 1923.

[29] O. Stern. Ein Weg zur experimentellen Prüfung der Richtungsquantelung im Magnetfeld. *Z. Phys.*, 7:249, 1921.

[30] W. Gerlach and O. Stern. Der experimentelle Nachweis des magnetischen Moments des Silberatoms. *Z. Phys.*, 8:110, 1921.

[31] W. Gerlach and O. Stern. Der experimentelle Nachweis der Richtungsquantelung im Magnetfeld. *Z. Phys.*, 9:349, 1922.

[32] A. H. Compton. Possible magnetic polarity of free electrons. *Philos. Mag.*, 41:279, 1921.

[33] W. Heisenberg. Über quantentheoretische Umdeutung kinematischer und mechanischer Beziehungen. *Z. Phys.*, 33:879, 1925.

[34] M. Born and P. Jordan. Zur Quantenmechanik. *Z. Phys.*, 34:858, 1925.

[35] M. Born, W. Heisenberg, and P. Jordan. Zur Quantenmechanik. II. *Z. Phys.*, 35:557, 1926.

[36] E. Schrödinger. Quantisierung als Eigenwertproblem. Erste Mitteilung. *Ann. Phys.*, 384:361, 1926.

[37] E. Schrödinger. Quantisierung als Eigenwertproblem. Zweite Mitteilung. *Ann. Phys.*, 384:489, 1926.

[38] E. Schrödinger. Quantisierung als Eigenwertproblem. Dritte Mitteilung. *Ann. Phys.*, 385:437, 1926.

[39] E. Schrödinger. Quantisierung als Eigenwertproblem. Vierte Mitteilung. *Ann. Phys.*, 386:109, 1926.

[40] L. deBroglie. Waves and Quanta. *Nature*, 112:540, 1923.

[41] E. Schrödinger. Über das Verhältnis der Heisenberg-Born-Jordanschen Quantenmechanik zu der meinem. *Ann. Phys.*, 384:734, 1926.

[42] P. M. A. Dirac. On the Theory of Quantum Mechanics. *Proc. R. Soc. London, Ser. A*, 112:661, 1926.

[43] J. von Neumann. *Mathematische Grundlagen der Quantenmechanik*. Springer Verlag Berlin, 1932.

[44] W. Pauli. Zur Quantenmechanik des magnetischen Elektrons. *Z. Phys.*, 43:601, 1927.

[45] P. M. A. Dirac. The Quantum Theory of the Electron. *Proc. R. Soc. London, Ser. A*, 117:610, 1928.

[46] P. M. A. Dirac. The Quantum Theory of the Electron. Part II. *Proc. R. Soc. London, Ser. A*, 118:351, 1928.

[47] P. W. Anderson. More Is Different - Broken symmetry and the nature of the hierarchical structure of science. *Science*, 177:393, 1972.

[48] S. Goudsmit and G. E. Uhlenbeck. Die Kopplungsmöglichkeiten der Quantenvektoren im Atom. *Z. Phys.*, 35:618, 1925.

[49] W. Pauli. Über den Zusammenhang des Abschlusses der Elektronengruppen im Atom mit der Komplexstruktur der Spektren. *Z. Phys.*, 31:765, 1925.

[50] E. Fermi. Zur Quantelung des idealen einatomigen Gases. *Z. Phys.*, 36:902, 1926.

[51] W. Pauli. Über Gasentartung und Paramagnetismus. *Z. Phys.*, 41:81, 1927.

[52] A. Sommerfeld. Zur Elektronentheorie der Metalle auf Grund der Fermischen Statistik. I. Teil: Allgemeines, Strömungs- und Austrittsvorgänge. *Z. Phys.*, 47:1, 1928.

[53] A. Sommerfeld. Zur Elektronentheorie der Metalle auf Grund der Fermischen Statistik. II. Teil: Thermoelektrische, galvanomagnetische und thermomagnetische Vorgänge. *Z. Phys.*, 47:43, 1928.

[54] H. Bethe. Theorie der Beugung von Elektronen an Kristallen. *Ann. Phys.*, 392:55, 1928.

[55] E. E. Witmer and L. Rosenfeld. Über die Beugung von de Broglieschen Wellen an Kristallgittern. *Z. Phys.*, 48:530, 1928.

[56] F. Bloch. Über die Quantenmechanik der Elektronen in Kristallgittern. *Z. Phys.*, 52:555, 1929.

[57] R. Peierls. Zur Theorie der galvanomagnetischen Effekte. *Z. Phys.*, 53:255, 1929.

[58] R. Peierls. Zur Theorie der elektrischen und thermischen Leitfähigkeit von Metallen. *Ann. Phys.*, 396:121, 1930.

[59] A. H. Wilson. The Theory of Electronic Semi-Conductors. *Proc. R. Soc. London, Ser. A*, 133:458, 1931.

[60] A. H. Wilson. The Theory of Electronic Semi-Conductors. II. *Proc. R. Soc. London, Ser. A*, 134:277, 1931.

[61] E. Wigner and F. Seitz. On the Constitution of Metallic Sodium. *Phys. Rev.*, 43:804, 1933.

[62] E. Wigner and F. Seitz. On the Constitution of Metallic Sodium. II. *Phys. Rev.*, 46:509, 1934.

[63] J. C. Slater. Electronic energy bands in metals. *Phys. Rev.*, 45:794, 1934.

[64] R. M. Martin. *Electronic Structure - Basic Theory and Practical Methods*. Cambridge University Press, 2004.

[65] E. Fues. Die Berechnung wasserstoffunähnlicher Spektren aus Zentralbewegungen der Elektronen. I. *Z. Phys.*, 11:364, 1922.

[66] E. Fues. Die Berechnung wasserstoffunähnlicher Spektren aus Zentralbewegungen der Elektronen II. *Z. Phys.*, 12:1, 1923.

[67] L. H. Thomas. The calculation of atomic fields. *Proc. Cambridge Philos. Soc.*, 23:542, 1927.

[68] E. Fermi. Un metodo statistico per la determinazione di alcune priorieta dell'atome. *Rend. Accad. Naz. Lincei*, 6:602, 1927.

[69] P. Hohenberg and W. Kohn. Inhomogeneous Electron Gas. *Phys. Rev.*, 136:B864, 1964.

[70] W. Kohn and L. Sham. Self-Consistent Equations Including Exchange and Correlation Effects. *Phys. Rev.*, 140:A1133, 1965.

[71] A. D. Becke. Density-functional thermochemistry. III. The role of exact exchange. *J. Chem. Phys.*, 98:5648, 1993.

[72] A. D. Becke. Density-functional exchange-energy approximation with correct asymptotic behavior. *Phys. Rev. A*, 38:3098, 1988.

[73] J. P. Perdew, J. A. Chevary, S. H. Vosko, K. A. Jackson, M. R. Pederson, D. J. Singh, and C. Fiolhais. Atoms, molecules, solids, and surfaces: Applications of the generalized gradient approximation for exchange and correlation. *Phys. Rev. B*, 46:6671, 1992.

[74] J. P. Perdew and K. Schmidt. Jacob's ladder of density functional approximations for the exchange-correlation energy. *AIP Conf. Proc.*, 577:1, 2001.

[75] J. P. Perdew. Accurate density functional for the energy: Real-space cutoff of the gradient expansion for the exchange hole. *Phys. Rev. Lett.*, 55:1665, 1985.

[76] J. P. Perdew. Erratum: Accurate density functional for the energy: Real-space cutoff of the gradient expansion for the exchange hole [Phys. Rev. Lett. 55, 1665 (1985)]. *Phys. Rev. Lett.*, 55:2370, 1985.

[77] W. M. Haynes, editor. *Handbook of Chemistry and Physics, 91st Edition*. CRC press, Cleveland, Ohio, 91 edition, 2010.

[78] B. Simard, P. A. Hackett, A. M. James, and P. R. R. Langridge-Smith. The bond length of silver dimer. *Chem. Phys. Lett.*, 186:415, 1991.

[79] R. S. Fellers, C. Leforestier, L. B. Braly, M. G. Brown, and R. J. Saykally. Spectroscopic determination of the water pair potential. *Science*, 284:945, 1999.

[80] J. P. Perdew, K. Burke, and M. Ernzerhof. Generalized gradient approximation made simple. *Phys. Rev. Lett.*, 77:3865, 1996.

[81] B. Hammer, L. B. Hansen, and J. K. Nørskov. Improved adsorption energetics within density-functional theory using revised Perdew-Burke-Ernzerhof functionals. *Phys. Rev. B*, 59:7413, 1999.

[82] J. D. van der Waals. *On the Continuity of the Gaseous and Liquid States*, volume XIV of *Studies in Statistical Mechanics*. North-Holland Physics Publishing, Amsterdam, The Netherlands, 1988.

[83] W. H. Keesom. On Waal's cohesion forces. *Phys. Z.*, 22:129, 1921.

[84] W. H. Keesom. Van der Waals's cohesion strength - Correction. *Phys. Z.*, 22:643, 1921.

[85] P. Debye. Van der Waals cohesion forces. *Phys. Zeits.*, 21:178, 1920.

[86] R. Eisenschitz and F. London. Über das Verhältnis der van der Waalsschen Kräfte zu den homöopolaren Bindungskräften. *Z. Phys.*, 60:491, 1930.

[87] F. London. Zur Theorie und Systematik der Molekularkräfte. *Z. Phys.*, 63:245, 1930.

[88] D. C. Langreth, B. I. Lundqvist, S. D. Chakarova-Käck, V. R. Cooper, M. Dion, P. Hyldgaard, A. Kelkkanen, J. Kleis, L. Kong, and S. Li. A density functional for sparse matter. *J. Phys. Condens. Matter*, 21:084203, 2009.

[89] P. Lazić, N. Atodiresei, M. Alaei, V. Caciuc, and S. Blügel. JuNoLo – Jülich nonlocal code for parallel post-processing evaluation of vdW-DF correlation energy. *Comput. Phys. Commun.*, 181:371, 2010.

[90] H. Rydberg, M. Dion, N. Jacobson, E. Schröder, P. Hyldgaard, S. Simak, D. Langreth, and B. Lundqvist. Van der Waals Density Functional for Layered Structures. *Phys. Rev. Lett.*, 91:126402, 2003.

[91] M. Dion, H. Rydberg, E. Schröder, D. Langreth, and B. Lundqvist. Van der Waals Density Functional for General Geometries. *Phys. Rev. Lett.*, 92:246401, 2004.

[92] M. Dion, H. Rydberg, E. Schröder, D. Langreth, and B. Lundqvist. Erratum: Van der Waals Density Functional for General Geometries [Phys. Rev. Lett. 92, 246401 (2004)]. *Phys. Rev. Lett.*, 95:109902, 2005.

[93] T. Thonhauser, V. R. Cooper, S. Li, A. Puzder, P. Hyldgaard, and D. C. Langreth. Van der Waals density functional: Self-consistent potential and the nature of the van der Waals bond. *Phys. Rev. B*, 76:125112, 2007.

[94] D. C. Langreth, M. Dion, H. Rydberg, E. Schröder, P. Hyldgaard, and B. I. Lundqvist. Van der Waals density functional theory with applications. *Int. J. Quant. Chem.*, 101:599, 2005.

[95] H. Rydberg, B. I. Lundqvist, D. C. Langreth, and M. Dion. Tractable nonlocal correlation density functionals for flat surfaces and slabs. *Phys. Rev. B*, 62:6997, 2000.

[96] F. Ortmann, W. G. Schmidt, and F. Bechstedt. Attracted by long-range electron correlation: adenine on graphite. *Phys. Rev. Lett.*, 95:186101, 2005.

[97] F. Ortmann, F. Bechstedt, and W. G. Schmidt. Semiempirical van der Waals correction to the density functional description of solids and molecular structures. *Phys. Rev. B*, 73:205101, 2006.

[98] S. Grimme. Semiempirical GGA-type density functional constructed with a long-range dispersion correction. *J. Comput. Chem.*, 27:1787, 2006.

[99] T. Bucko, J. Hafner, S. Lebègue, and J. G. Angyàn. Improved Description of the Structure of Molecular and Layered Crystals: Ab Initio DFT Calculations with van der Waals Corrections. *J. Phys. Chem. A*, 114:11814, 2010.

[100] M. Rohlfing and T. Bredow. Binding Energy of Adsorbates on a Noble-Metal Surface: Exchange and Correlation Effects. *Phys. Rev. Lett.*, 101:266106, 2008.

[101] L. Romaner, D. Nabok, P. Puschnig, E. Zojer, and C. Ambrosch-Draxl. Theoretical study of PTCDA adsorbed on the coinage metal surfaces, Ag(111), Au(111) and Cu(111). *New J. Phys.*, 11:053010, 2009.

[102] G. Mercurio, E. R. McNellis, I. Martin, S. Hagen, F. Leyssner, S. Soubatch, J. Meyer, M. Wolf, P. Tegeder, F. S. Tautz, and K. Reuter. Structure and Energetics of Azobenzene on Ag(111): Benchmarking Semiempirical Dispersion Correction Approaches. *Phys. Rev. Lett.*, 104:036102, 2010.

[103] E. Rauls, S. Blankenburg, and W. G. Schmidt. Chemical reactivity on surfaces: Modeling the imide synthesis from DATP and PTCDA on Au (111). *Phys. Rev. B*, 81:125401, 2010.

[104] S. Lebègue, J. Harl, T. Gould, J. G. Angyàn, G. Kresse, and J. F. Dobson. Cohesive properties and asymptotics of the dispersion interaction in graphite by the random phase approximation. *Accepted in Phys. Rev. Lett.*, 2010.

[105] P. E. Blöchl. Projector augmented-wave method. *Phys. Rev. B*, 50:17953, 1994.

[106] O. K. Andersen. Linear methods in band theory. *Phys. Rev. B*, 12:3060, 1975.

[107] D. R. Hamann, M. Schlüter, and C. Chiang. Norm-conserving pseudopotentials. *Phys. Rev. Lett.*, 43:1494, 1979.

[108] G. Kresse and J. Furthmüller. Efficient iterative schemes for ab initio total-energy calculations using a plane-wave basis set. *Phys. Rev. B*, 54:11169, 1996.

[109] G. Kresse and J. Furthmüller. Efficiency of ab-initio total energy calculations for metals and semiconductors using a plane-wave basis set. *Comput. Mater. Sci*, 6:15, 1996.

[110] G. Kresse and D. Joubert. From ultrasoft pseudopotentials to the projector augmented-wave method. *Phys. Rev. B*, 59:1758, 1999.

[111] R. Car and M. Parrinello. Unified approach for molecular dynamics and density-functional theory. *Phys. Rev. Lett.*, 55:2471, 1985.

[112] P. Ehrenfest. Bemerkung über die angenäherte Gültigkeit der klassischen Mechanik innerhalb der Quantenmechanik. *Z. Phys.*, 45:455, 1927.

[113] H. Hellmann. *Einführung in die Quantenchemie*. Deuticke, Leipzig, 1937.

[114] R. P. Feynman. Forces in molecules. *Phys. Rev.*, 56:340, 1939.

[115] A. Sanchez, S. Abbet, U. Heiz, W. D. Schneider, H. Häkkinen, R. N. Barnett, and U. Landman. When gold is not noble: Nanoscale gold catalysts. *J. Phys. Chem. A*, 103:9573, 1999.

[116] A. Bongiorno and U. Landman. Water-Enhanced Catalysis of CO oxidation on Free and Supported Gold Nanoclusters. *Phys. Rev. Lett.*, 95:106102, 2005.

[117] O. Echt, K. Sattler, and E. Recknagel. Magic numbers for sphere packings: experimental verification in free xenon clusters. *Phys. Rev. Lett.*, 47:1121, 1981.

[118] M. Piotrowski, P. Piquini, and J. Da Silva. Density functional theory investigation of 3d, 4d, and 5d 13-atom metal clusters. *Phys. Rev. B*, 81:155446, 2010.

[119] K. S. Novoselov, A. K. Geim, S. V. Morozov, D. Jiang, Y. Zhang, S. V. Dubonos, I. V. Grigorieva, and A. A. Firsov. Electric field effect in atomically thin carbon films. *Science*, 306:666, 2004.

[120] K. S. Novoselov, A. K. Geim, S. V. Morozov, D. Jiang, M. I. Katsnelson I. V. Grigorieva, S. V. Dubonos, and A. A. Firsov. Two-dimensional gas of massless Dirac fermions in graphene. *Nature*, 438:197, 2005.

[121] K. S. Novoselov, D. Jiang, F. Schedin, T. J. Booth, V. V. Khotkevich, S. V. Morozov, and A. K. Geim. Two-dimensional atomic crystals. *PNAS*, 102:10451, 2005.

[122] A. K. Geim and K. S. Novoselov. The rise of graphene. *Nat. Mater.*, 6:183, 2007.

[123] M. I. Katsnelson. Graphene: carbon in two dimensions. *Mater. today*, 10:20, 2007.

[124] A. K. Geim. Graphene: status and prospects. *Science*, 324:1530, 2009.

[125] Z. Luo, L. A. Somers, Y. Dan, T. Ly, N. J. Kybert, E. J Mele, and A. T. C. Johnson. Size-Selective Nanoparticle Growth on Few-Layer Graphene Films. *Nano Lett.*, 10:777, 2010.

[126] J. J. Rehr, E. Zaremba, and W. Kohn. van der Waals forces in noble metals. *Phys. Rev. B*, 12:2062, 1975.

[127] J. P. Perdew and A. Zunger. Self-interaction correction to density-functional approximations for many-electron systems. *Phys. Rev. B*, 23:5048, 1981.

[128] W. Tang, E. Sanville, and G. Henkelman. A Grid-Based Bader Analysis Algorithm without Lattice Bias. *J. Phys. Condens. Matter*, 21:084204, 2009.

[129] J. J. Berzelius. Einige Ideen über eine bei der Bildung organischer Verbindungen in der lebenden Natur wirksame, aber bisher nicht bemerkte Kraft. *Jahresberichte über die Fortschritte der physischen Wissenschaften, Dt. Übersetzung*, page 237, 1836.

[130] W. Ostwald. Definition der Katalyse. *Z. Phys. Chem.*, 15:706, 1894.

[131] C. Joachim and L. Plévert. *Nanosciences: the invisible revolution*. World Scientific Publishing, Singapore, 2009.

[132] U. Heiz and U. Landman, editors. *Nanocatalysis*. Springer-Verlag, Berlin, Heidelberg, 2007.

[133] M. Haruta, T. Kobayashi, H. Sano, and N. Yamada. Novel Gold Catalysts for the Oxidation of Carbon Monoxide at a Temperature far Below 0° C. *Chem. Lett.*, 16:405, 1987.

[134] J. W. Döbereiner. *Ann. Chim. Phys.*, 24:91, 1823.

[135] P. L. Dulong and L. G. Thenard. *Ann. Chim. Phys.*, 23:440, 1823.

[136] G. Bond. The Early History of Catalysis by Gold - A review of the literature before 1978. *Gold Bull.*, 41:235, 2008.

[137] G. Bond and D. Thompson. Catalysis by gold. *Catal. Rev. Sci. Eng.*, 41:319, 1999.

[138] M. Haruta and M. Date. Advances in the catalysis of Au nanoparticles. *Appl. Catal., A*, 222:427, 2001.

[139] A. Hashmi and G. Hutchings. Gold Catalysis. *Angew. Chem. Int. Ed.*, 45:7896, 2006.

[140] B. Hvolbæk, T. Janssens, and B. Clausen. Catalytic activity of Au nanoparticles. *Nano Today*, 2:14, 2007.

[141] P. Pyykkö. Theoretical Chemistry of Gold. *Angew. Chem. Int. Ed.*, 43:4412, 2004.

[142] P. Pyykkö. Theoretical Chemistry of Gold. II. *Inorg. Chim. Acta*, 358:4113, 2005.

[143] P. Pyykkö. Theoretical Chemistry of Gold. III. *Chem. Soc. Rev.*, 37:1967, 2008.

[144] S. Lee, G. Apai, M. Mason, R. Benbow, and Z. Hurych. Evolution of band structure in gold clusters as studied by photoemission. *Phys. Rev. B*, 23:505, 1981.

[145] J. Callaway. Clusters of transition-metal atoms. *Chem. Rev.*, 86:1049, 1986.

[146] J. Ho, K. M. Ervin, and W. C. Lineberger. Photoelectron spectroscopy of metal cluster anions: Cu_n^-, Ag_n^-, and Au_n^-. *J. Chem. Phys.*, 93:6987, 1990.

[147] K. J. Taylor, C. L. Pettiette-Hall, O. Cheshnovsky, and R. E. Smalley. Ultraviolet photoelectron spectra of coinage metal clusters. *J. Chem. Phys.*, 96:3319, 1992.

[148] C. L. Cleveland, U. Landman, T. G. Schaaff, M. N. Shafigullin, P. W. Stephens, and R. L. Whetten. Structural evolution of smaller gold nanocrystals: The truncated decahedral motif. *Phys. Rev. Lett.*, 79:1873, 1997.

[149] O. Häberlen, S. Chung, M. Stener, and N. Rösch. From clusters to bulk: A relativistic density functional investigation on a series of gold clusters Au_n, n = 6, ... ,147. *J. Chem. Phys.*, 106:5189, 1997.

[150] H. Häkkinen and U. Landman. Gold clusters (Au_N, 2<= N<= 10) and their anions. *Phys. Rev. B*, 62:R2287, 2000.

[151] H. Grönbeck and W. Andreoni. Gold and platinum microclusters and their anions: comparison of structural and electronic properties. *Chem. Phys.*, 262:1, 2000.

[152] H. Häkkinen, M. Moseler, and U. Landman. Bonding in Cu, Ag, and Au clusters: relativistic effects, trends, and surprises. *Phys. Rev. Lett.*, 89:33401, 2002.

[153] J. Oviedo and R. E. Palmer. Amorphous structures of Cu, Ag, and Au nanoclusters from first principles calculations. *J. Chem. Phys.*, 117:9548, 2002.

[154] J. Wang, G. Wang, and J. Zhao. Density-functional study of Au_n (n=2-20) clusters: Lowest-energy structures and electronic properties. *Phys. Rev. B*, 66:035418, 2002.

[155] J. Li, X. Li, H. J. Zhai, and L. S. Wang. Au_{20}: A Tetrahedral Cluster. *Science*, 299:864, 2003.

[156] B. Soulé De Bas, M. Ford, and M. Cortie. Low energy structures of gold nanoclusters in the size range 3-38 atoms. *J. Mol. Struct. THEOCHEM*, 686:193, 2004.

[157] L. Xiao, B. Tollberg, X. Hu, and L. Wang. Structural study of gold clusters. *J. Chem. Phys.*, 124:114309, 2006.

[158] P. Pyykkö. Relativistic effects in structural chemistry. *Chem. Rev.*, 88:563, 1988.

[159] Y. Shen and J. BelBruno. Density Functional Theory Study of the Jahn-Teller Effect and Spin-Orbit Coupling for Copper and Gold Trimers. *J. Phys. Chem. A*, 109:512, 2005.

[160] X. Yang, J. Zhou, H. Weng, and J. Dong. Spin-orbit interaction in Au structures of various dimensionalities. *Appl. Phys. Lett.*, 92:023115, 2008.

[161] B. Molina, J. R. Soto, and A. Calles. Competition between Jahn-Teller effect and spin-orbit coupling in t_d $Au_{20}^{\pm\gamma}$ γ = 1,2,3. *Eur. Phys. J. D*, 51:225, 2009.

[162] H. Häkkinen and U. Landman. Gas-Phase Catalytic Oxidation of CO by Au_2^-. *JACS*, 123:9704, 2001.

[163] J. Hagen, L. D. Socaciu, M. Elijazyfer, U. Heiz, T. M. Bernhardt, and L. Wöste. Coadsorption of CO and O_2 on small free gold cluster anions at cryogenic temperatures: Model complexes for catalytic CO oxidation. *Phys. Chem. Chem. Phys.*, 4:1707, 2002.

[164] L. D. Socaciu, J. Hagen, T. M. Bernhardt, L. Wöste, U. Heiz, H. Häkkinen, and U. Landman. Catalytic CO Oxidation by Free Au_2^-: Experiment and Theory. *JACS*, 125:10437, 2003.

[165] N. Lopez, J. K. Nørskov, T. V. W. Janssens, A. Carlsson, A. Puig-Molina, B. S. Clausen, and J. D. Grunwaldt. The adhesion and shape of nanosized Au particles in a Au/TiO_2 catalyst. *J. Catal.*, 225:86, 2004.

[166] T. Janssens, B. Clausen, B. Hvolbæk, H. Falsig, C. H. Christensen, T. Bligaard, and J. K. Nørskov. Insights into the reactivity of supported Au nanoparticles: combining theory and experiments. *Top. Catal.*, 44:15, 2007.

[167] L. M. Molina and B. Hammer. Active Role of Oxide Support during CO Oxidation at Au/MgO. *Phys. Rev. Lett.*, 90:206102, 2003.

[168] L. M. Molina and B. Hammer. Theoretical study of CO oxidation on Au nanoparticles supported by MgO (100). *Phys. Rev. B*, 69:155424, 2004.

[169] B. Yoon, H. Häkkinen, U. Landman, A. S. Wörz, J. M. Antonietti, S. Abbet, K. Judai, and U. Heiz. Charging Effects on Bonding and Catalyzed Oxidation of CO on Au_8 Clusters on MgO. *Science*, 307:403, 2005.

[170] A. Ramos, R. Arratia-Perez, and G. Malli. Dirac scattered-wave calculations on an icosahedral Au_{13} cluster. *Phys. Rev. B*, 35:3790, 1987.

[171] R. Arratia-Perez, A. F. Ramos, and G. L. Malli. Calculated electronic structure of Au_{13} clusters. *Phys. Rev. B*, 39:3005, 1989.

[172] D. Wales and L. Munro. Changes of Morphology and Capping of Model Transition Metal Clusters. *J. Phys. Chem*, 100:2053, 1996.

[173] L. Lamare and F. Michel-Calendini. LDA electronic structure calculations on Au_{13} cluster. *Int. J. Quant. Chem.*, 61:635, 1997.

[174] Y. Sun, M. Zhang, and R. Fournier. Periodic trends in the geometric structures of 13-atom metal clusters. *Phys. Rev. B*, 77:75435, 2008.

[175] C. M. Chang and M. Y. Chou. Alternative low-symmetry structure for 13-atom metal clusters. *Phys. Rev. Lett.*, 93:133401, 2004.

[176] H. Häkkinen, B. Yoon, U. Landman, X. Li, H. J. Zhai, and L. S. Wang. On the Electronic and Atomic Structures of Small Au_N^- (n = 4 - 14) Clusters: A Photoelectron Spectroscopy and Density-Functional Study. *J. Phys. Chem. A*, 107:6168, 2003.

[177] M. Gruber, G. Heimel, L. Romaner, J.-L. Brédas, and E. Zojer. First-principles study of the geometric and electronic structure of Au_{13} clusters: Importance of the prism motif. *Phys. Rev. B*, 77:165411, 2008.

[178] A. Vargas, G. Santarossa, M. Iannuzzi, and A. Baiker. Fluxionality of gold nanoparticles investigated by Born-Oppenheimer molecular dynamics. *Phys. Rev. B*, 80:195421, 2009.

[179] L. Xiao and L. Wang. From planar to three-dimensional structural transition in gold clusters and the spin-orbit coupling effect. *Chem. Phys. Lett.*, 392:452, 2004.

[180] M. Okumura, Y. Kitagawa, and M. Haruta. DFT studies of interaction between O_2 and Au clusters. The role of anionic surface Au atoms .... *Chem. Phys. Lett.*, 346:163, 2001.

[181] M. Okumura, Y. Kitagawa, and M. Haruta. The interaction of neutral and charged Au clusters with O_2, CO and H_2. *Appl. Catal., A*, 291:37, 2005.

[182] A. Prestianni, A. Martorana, F. Labat, and I. Ciofini. Theoretical Insights on O_2 and CO Adsorption on Neutral and Positively Charged Gold Clusters. *J. Phys. Chem. B*, 110:12240, 2006.

[183] B. Wells and A. Chaffee. Gas binding to Au_{13}, $Au_{12}Pd$, and $Au_{11}Pd_2$ nanoclusters in the context of catalytic oxidation and reduction reactions. *J. Chem. Phys.*, 129:164712, 2008.

[184] A. Prestianni, A. Martorana, I. Ciofini, F. Labat, and C. Adamo. CO Oxidation on Cationic Gold Clusters: A Theoretical Study. *J. Chem. Phys. C*, 112:18061, 2008.

[185] A. Prestianni, A. Martorana, F. Labat, I. Ciofini, and C. Adamo. A DFT investigation of CO oxidation over neutral and cationic gold clusters. *J. Mol. Struct. THEOCHEM*, 903:34, 2009.

[186] A. H. Castro-Neto, N. M. R. Peres, K. S. Novoselov, and A. K. Geim. The electronic properties of graphene. *Rev. Mod. Phys.*, 81:109, 2009.

[187] M. I. Katsnelson, K. S. Novoselov, and A. K. Geim. Chiral tunnelling and the Klein paradox in graphene. *Nat. Phys.*, 2:620, 2006.

[188] K. S. Novoselov, Z. Jiang, Y. Zhang, S. V. Morozov, H. L. Stormer, U. Zeitler, J. C. Maan, G. S. Boebinger, P. Kim, and A. K. Geim. Room-Temperature Quantum Hall Effect in Graphene. *Science*, 315:1379, 2007.

[189] D. M. Duffy and J. A. Blackman. The Energy of Ag Adatoms and Dimers on Graphite. *Surf. Sci.*, 415:L1016, 1998.

[190] G. M. Wang, J. J. BelBruno, S. D. Kenny, and R. Smith. Interaction of Silver Adatoms and Dimers with Graphite Surfaces. *Surf. Sci.*, 541:91, 2003.

[191] A. Maiti and A. Ricca. Metal-Nanotube Interactions - Binding Energies and Wetting Properties. *Chem. Phys. Lett.*, 395:7, 2004.

[192] G. P. Brivio and M. I. Trioni. The adiabatic molecule-metal surface interaction: Theoretical approaches. *Rev. Mod. Phys.*, 71:231, 1999.

[193] T. P. Darby and C. M. Wayman. Growth of gold thin film dendrites on graphite substrates. *J. Cryst. Growth*, 29:98, 1975.

[194] P. Koskinen, H. Häkkinen, B. Huber, B. von Issendorff, and M. Moseler. Liquid-Liquid Phase Coexistence in Gold Clusters: 2D or Not 2D? *Phys. Rev. Lett*, 98:015701, 2007.

[195] R. Olson, S. Varganov, M. Gordon, and H. Metiu. Where does the planar-to-nonplanar turnover occur in small gold clusters? *JACS*, 127:1049, 2005.

Acta Universitatis Upsaliensis

Digital Comprehensive Summaries of Uppsala Dissertations from the Faculty of Science and Technology 788

Editor: The Dean of the Faculty of Science and Technology

A doctoral dissertation from the Faculty of Science and Technology, Uppsala University, is usually a summary of a number of papers. A few copies of the complete dissertation are kept at major Swedish research libraries, while the summary alone is distributed internationally through the series Digital Comprehensive Summaries of Uppsala Dissertations from the Faculty of Science and Technology. (Prior to January, 2005, the series was published under the title "Comprehensive Summaries of Uppsala Dissertations from the Faculty of Science and Technology".)

Distribution: publications.uu.se
urn:nbn:se:uu:diva-133246

ACTA
UNIVERSITATIS
UPSALIENSIS
UPPSALA
2010